

การวิเคราะห์วัสดุเชิงประกอบเสริมด้วยเส้นใยโพลีไซอิดเล็กทริกที่มีความบกพร่องของรอยต่อ

นาย ยโสธร ทรัพย์เสถียร

วิทยานิพนธ์นี้เป็นส่วนหนึ่งของการศึกษาตามหลักสูตรปริญญาวิศวกรรมศาสตรดุษฎีบัณฑิต

สาขาวิชาวิศวกรรมโยธา ภาควิชาวิศวกรรมโยธา

คณะ วิศวกรรมศาสตร์ จุฬาลงกรณ์มหาวิทยาลัย

ปีการศึกษา 2551

ลิขสิทธิ์ของจุฬาลงกรณ์มหาวิทยาลัย

ANALYSIS OF PIEZOELECTRIC FIBER-REINFORCED COMPOSITES  
WITH IMPERFECT INTERFACE

Mr.Yasothorn Sapsathiam

A Dissertation Submitted in Partial Fulfillment of the Requirements  
for the Degree of Doctor of Philosophy Program in Civil Engineering

Department of Civil Engineering

Faculty of Engineering

Chulalongkorn University

Academic year 2008

Copyright of Chulalongkorn University



ยโสธร ทรัพย์เสถียร : การวิเคราะห์วัสดุเชิงประกอบเสริมด้วยเส้นใยไพเอโซอิเล็กทริกที่มีความบกพร่องของรอยต่อ. (ANALYSIS OF PIEZOELECTRIC FIBER-REINFORCED COMPOSITES WITH IMPERFECT INTERFACE) อ.ที่ปรึกษา  
วิทยานิพนธ์หลัก : รศ.ดร.ธีรพงศ์ เสนจันทร์มิไชย, 80 หน้า.

วิทยานิพนธ์ฉบับนี้เกี่ยวข้องกับทฤษฎีและการวิเคราะห์และศึกษาพฤติกรรมของวัสดุเชิงประกอบเสริมด้วยเส้นใยไพเอโซอิเล็กทริกซึ่งถูกนำไปประยุกต์ใช้งานอย่างแพร่หลายเนื่องจากวัสดุประเภทนี้มีความสามารถในการตอบสนองทางกลควบคู่กับการตอบสนองทางไฟฟ้า งานวิจัยนี้ใช้วิธีการแปลงฟูเรียร์เพื่อวิเคราะห์หาค่าตอบทั่วไปสำหรับวัสดุไพเอโซอิเล็กทริกที่มีความสมมาตรกับแนวแกน ค่าตอบทั่วไปที่หาได้ดังกล่าว สามารถนำมาใช้วิเคราะห์พฤติกรรม การถ่ายแรงภายในวัสดุเชิงประกอบเสริมด้วยเส้นใยไพเอโซอิเล็กทริกและพฤติกรรมของวัสดุเชิงประกอบที่มีรอยแตกที่รอยต่อระหว่างเส้นใยไพเอโซอิเล็กทริกและวัสดุหลักอิลาสติกได้ งานวิจัยนี้ทำการวิเคราะห์พฤติกรรมการถ่ายแรงของวัสดุเชิงประกอบเสริมด้วยเส้นใยไพเอโซอิเล็กทริกภายใต้แรงกระทำทั้งทางกลและทางไฟฟ้า โดยพิจารณาทั้งกรณีวัสดุเสริมและวัสดุหลักของวัสดุเชิงประกอบมีการยึดติดกันแบบสมบูรณ์และแบบไม่สมบูรณ์ รวมทั้งพิจารณาเงื่อนไขขอบเขตทางไฟฟ้าทั้งชนิดวงจรปิดและวงจรเปิด และศึกษารณที่มีรอยแตกที่รอยต่อระหว่างเส้นใยไพเอโซอิเล็กทริกและวัสดุหลักโดยประยุกต์ใช้วิธีการเคลื่อนที่ไม่ต่อเนื่อง (Displacement Discontinuity Method) จากนั้นได้พัฒนาโปรแกรมเพื่อใช้ในการคำนวณผลเชิงตัวเลขสำหรับปัญหาการถ่ายแรงและปัญหารอยแตกที่รอยต่อระหว่างเส้นใยไพเอโซอิเล็กทริกกับวัสดุหลักอิลาสติก จากผลการศึกษาที่เสนอในวิทยานิพนธ์ฉบับนี้พบว่า ลักษณะและประเภทของแรงกระทำ คุณสมบัติของเส้นใย ไพเอโซอิเล็กทริก คุณสมบัติของวัสดุหลักอิลาสติก การเกิดรอยแตกที่รอยต่อ รวมทั้งชนิดของขอบเขตทางไฟฟ้า มีผลต่อพฤติกรรมของวัสดุเชิงประกอบเสริมด้วยเส้นใยไพเอโซอิเล็กทริกอย่างมาก นอกจากนี้ยังพบว่าเมื่อเส้นใยไพเอโซอิเล็กทริกยึดติดกับวัสดุหลักแบบไม่สมบูรณ์ จะเกิดการถ่ายแรงจากวัสดุเส้นใยไพเอโซอิเล็กทริกไปยังวัสดุหลักน้อยลง ซึ่งส่งผลทำให้หน่วยแรงที่เกิดขึ้นจากการถ่ายแรงระหว่างเส้นใยไพเอโซอิเล็กทริกกับวัสดุหลักที่รอยต่อลดลงด้วย องค์ความรู้ที่ได้จากงานวิจัยนี้มีประโยชน์ต่อการออกแบบและพัฒนาวัสดุเชิงประกอบประเภทนี้ให้มีคุณสมบัติเหมาะสมกับการประยุกต์ใช้ในงานประเภทต่างๆ ได้ดีขึ้น

ภาควิชา.....วิศวกรรมโยธา..... ลายมือชื่อนิสิต.....  
สาขาวิชา.....วิศวกรรมโยธา..... ลายมือชื่ออ.ที่ปรึกษาวิทยานิพนธ์หลัก.....  
ปีการศึกษา.....2551.....

# # 4771844821 : MAJOR CIVIL ENGINEERING

KEYWORDS : PIEZOELECTRICITY / COMPOSITE MATERIALS / IMPERFECT  
INTERFACE / LOAD TRANSFER / CYLINDRICAL CRACK

YASOTHORN SAPSATHIARN : ANALYSIS OF PIEZOELECTRIC FIBER-  
REINFORCED COMPOSITES WITH IMPERFECT INTERFACE. ADVISOR :  
TEERAPONG SENJUNTICHAJ, Ph.D., 80 pp.

This thesis is concerned with the study of the electroelastic responses in piezoelectric fiber-reinforced composites which are widely used in as sensors and actuators due to their intrinsic electro-mechanical coupling properties. General solutions corresponding to an infinite piezoelectric fiber with a vertical body force and an infinite transversely isotropic elastic medium with a cylindrical hole are derived by using Fourier integral transforms. These general solutions are used to solve the mechanical load and electric charge transfer from a cylindrical piezoelectric fiber into a surrounding transversely isotropic elastic matrix. The fiber-matrix interface is considered to be either mechanically perfect or imperfect and either electrically open- or short-circuited. The three-dimensional axisymmetric interfacial crack in a piezoelectric fiber-reinforced composite is also studied by employing the displacement discontinuity method (DDM) based on the fundamental solutions of interface dislocation. A computer program based on the above solution schemes has been developed. The validity and accuracy of the present solution scheme are confirmed by comparison with the existing solutions. Numerical results indicate that the electroelastic responses of a piezoelectric fiber-reinforced composite are very complicated and significantly influenced by properties of the piezoelectric fiber and the elastic matrix, electric boundary conditions and interface conditions. Compared to composites of BaTiO<sub>3</sub> and PZT-6B fibers, the electric field generated in PZT-4 fiber has the highest value implying that PZT-4 is more suitable for sensing applications. In addition, the presence of the imperfect interface results in lower axial load transfer to the matrix and hence lower interfacial stresses but a higher fiber vertical electrical field. A fundamental understanding obtained from the present study is very useful for a better design, development and application of 1-3piezocomposites with enhanced properties for advanced applications.

Department : CIVIL ENGINEERING Student's Signature : .....

Field of Study : CIVIL ENGINEERING Advisor's Signature : .....

Academic Year : 2008 .....

## ACKNOWLEDGEMENTS

This research work was supported by the Thailand Research Fund (TRF) under the Royal Golden Jubilee Ph.D. (RGJ-Ph.D.) scholarship and the 90th Anniversary of Chulalongkorn University Fund (Ratchadaphiseksomphot Endowment Fund). Their supports are gratefully acknowledged.

The author wishes to express his sincere appreciation to his advisor, Associate Professor Dr.Teerapong Senjuntichai for his kind guidance and long-term support throughout this work. He also wishes to express his gratitude to Professor Dr.Nimal Rajapakse at the University of British Columbia, Canada, for his kindness and invaluable advice on the research work and very warm welcome during the visit at UBC in 2007 and 2008. Grateful acknowledgements are due to Professor Dr.Thaksin Thepchatri, Associate Professor Dr.Pruettha Nanakorn, Assistant Professor Dr.Watanachai Smittakorn and Dr.Jaroon Rungamornrat for their helpful comments and serving in the thesis committee.

Special thanks are also due to everyone who has helped directly and indirectly in the preparation of this thesis. Finally, the author would like to express his gratitude to his parents for their support and love.

# CONTENTS

	page
Abstract (Thai) .....	iv
Abstract (English) .....	v
Acknowledgements .....	vi
Contents .....	vii
List of Tables.....	ix
List of Figures .....	x
List of Abbreviations .....	xiv
Chapter I Introduction.....	1
1.1 General .....	1
1.2 Objectives of Present Study .....	3
1.3 Scopes of Present Study .....	4
1.4 Basic Assumptions .....	4
Chapter II Literature Reviews.....	6
2.1 General.....	6
2.1 Fiber–Matrix Interaction .....	6
2.2 Cracks in Piezocomposites .....	8
Chapter III Basic Equations and General Solutions.....	11
3.1 Basic Equations.....	11
3.2 General Solutions of Piezoelectric Materials.....	13
3.2.1 Homogeneous Solution .....	14
3.2.2 Particular Solution .....	15
3.2.3 Complete General Solutions.....	16
3.3 General Solutions of Transversely Isotropic Elastic Materials .....	17

Chapter IV Electro–Mechanical Load Transfer in Piezocomposites .....	20
4.1 Problem Formulation .....	20
4.2 Numerical Results and Discussion .....	23
4.2.1 Comparison with Existing Solutions.....	23
4.2.2 Force and Charge Diffusion in Piezocomposites .....	24
Chapter V Cylindrical Interface Crack in Piezocomposites .....	45
5.1 Problem Formulation .....	45
5.1.1 Displacement Discontinuity Method (DDM) .....	46
5.1.2 Fundamental Solutions for Interface Dislocations .....	47
5.1.2.1 Radial Interface Dislocation .....	47
5.1.2.2 Axial Interface Dislocation .....	49
5.1.3 Order of Singularity and Field Intensity Factors .....	49
5.1.4 DDM Crack Tip Element.....	52
5.2 Numerical Results and Discussion .....	53
5.2.1 Comparison with Existing Solutions.....	54
5.2.2 Interface Cracks in Piezocomposites .....	55
Chapter VI Conclusions .....	64
6.1 Summary .....	64
6.2 Suggestions for Further Study on Piezocomposites .....	66
References.....	68
Appendices .....	75
Appendix A .....	76
Appendix B .....	78
Biography .....	80



## LIST OF TABLES

Table	page
Table 4.1 Material properties used in the numerical study .....	30
Table 5.1 Material properties used by Kasano et al. (1984) .....	57
Table A.1 Characteristic roots for piezoelectric materials .....	76
Table A.2 Characteristic roots for Matrix A and Matrix B .....	76

## LIST OF FIGURES

Figure	page
Figure 1.1 A 1–3 piezocomposite .....	5
Figure 3.1 A piezoelectric fiber–reinforced composite .....	19
Figure 4.1 A piezoelectric fiber–reinforced composite with imperfect interface.....	31
Figure 4.2 Comparison of the fiber axial force for elastic composites with perfect interface.....	31
Figure 4.3 Comparison of (a) fiber axial force; (b) interfacial shear stress and (c) interfacial radial stress for elastic composite with imperfect interface.....	32
Figure 4.4 (a) Resultant axial force and (b) vertical electric field along the $z$ –axis of piezoelectric fiber (open–circuited) under applied axial load.....	33
Figure 4.5 (a) Shear and (b) radial stresses along the fiber–matrix interface of piezoelectric composite (open–circuited) under applied axial load.....	34
Figure 4.6 (a) Vertical stress and (b) vertical electric field along the $z$ –axis of piezoelectric fiber (open–circuited) under applied electric charge. ....	35

Figure	page
Figure 4.7 (a) Shear and (b) radial stresses along the fiber–matrix interface of piezoelectric composite (open–circuited) under applied electric charge. ....	36
Figure 4.8 (a) Resultant axial force and (b) vertical electric field along the $z$ –axis of piezoelectric fiber (short–circuited) under applied axial load.....	37
Figure 4.9 (a) Vertical stress and (b) vertical electric field along the $z$ –axis of piezoelectric fiber (short–circuited) under applied electric charge. ....	38
Figure 4.10 (a) Shear stress profiles along the $r$ –axis at $z = 0$ and (b) radial stress profiles along the $r$ –axis at $z/a = 1$ (open–circuited) under applied axial load. ....	39
Figure 4.11 (a) Shear stress profiles along the $r$ –axis at $z = 0$ and (b) radial stress profiles along the $r$ –axis at $z/a = 1$ (open–circuited) under applied electric charge.....	40
Figure 4.12 Composite of PZT–6B fiber with Matrix A (a) resultant axial force and (b) vertical electric field along the $z$ –axis of piezoelectric fiber; (c) shear and (d) radial stresses along the fiber–matrix interface (open–circuited) under applied axial load for different interface stiffness values.....	41

Figure	page
Figure 4.13 Composite of PZT-4 fiber with Matrix B (a) resultant axial force and (b) vertical electric field along the $z$ -axis of piezoelectric fiber; (c) shear and (d) radial stresses along the fiber-matrix interface (open-circuited) under applied axial load for different interface stiffness values.....	42
Figure 4.14 Composite of PZT-6B fiber with Matrix A (a) vertical stress and (b) vertical electric field along the $z$ -axis of piezoelectric fiber; (c) shear and (d) radial stresses along the fiber-matrix interface of piezoelectric composite (open-circuited) under applied electric charge for different interface stiffness values. ....	43
Figure 4.15 Composite of PZT-4 fiber with Matrix B (a) vertical stress and (b) vertical electric field along the $z$ -axis of piezoelectric fiber; (c) shear and (d) radial stresses along the fiber-matrix interface of piezoelectric composite (open-circuited) under applied electric charge for different interface stiffness values. ....	44
Figure 5.1 A piezoelectric fiber-reinforced composite with interfacial crack. ....	58
Figure 5.2 Discretization of crack surface into $N$ segments. ....	58
Figure 5.3 A piezocomposite with an elemental displacement discontinuity element.....	59
Figure 5.4 DDM Crack tip element. ....	59

Figure	page
Figure 5.5 Comparison of crack opening displacement with cylindrical crack in elastic materials (a) $c/a = 10$ ; (b) $c/a = 1$ ; (c) $c/a = 0.1$ .....	60
Figure 5.6 Comparison of stress intensity factors for cylindrical crack in elastic materials.....	61
Figure 5.7 Comparison of stress intensity factors for cylindrical interface crack in elastic composite. ....	61
Figure 5.8 Crack opening displacements for cylindrical interface crack in piezocomposites with different $c/a$ (a) $c/a = 0.1$ ; (b) $c/a = 0.5$ ; (c) $c/a = 1.0$ ; (d) $c/a = 2.0$ ; (e) $c/a = 5.0$ ; (f) $c/a = 10.0$ . ....	62
Figure 5.9 Field intensity factors for cylindrical interface crack in piezocomposites. ....	63

## LIST OF ABBREVIATIONS

$a$	radius of a piezoelectric fiber;
$c$	half length of an interface crack;
$c_{ij}^f$	elastic constants of a piezoelectric fiber;
$c_{ij}^m$	elastic constants of an elastic matrix;
$D_i$	electric displacement vectors in the $i$ -direction;
$d_i$	displacement discontinuity in the $i$ -direction;
$E_i$	electric fields in the $i$ -direction;
$e_{ij}^f$	piezoelectric constants of a piezoelectric fiber;
$F_i$	body forces in the $i$ -direction;
$H$	Heaviside step function;
$I_n$	modified Bessel functions of the first kinds of order $n$ ;
$\hat{I}_n$	scaled modified Bessel functions of the first kinds of order $n$ ;
$K_D$	electric displacement intensity factor;
$K_I, K_{II}$	the first and second mode intensity factors;
$K_n$	modified Bessel functions of the second kinds of order $n$ ;
$\hat{K}_n$	scaled modified Bessel functions of the second kinds of order $n$ ;
$k_s$	spring-factor parameter;
$P$	resultant axial force in a piezoelectric fiber;
$P_0$	total magnitude of an applied axial force in a piezoelectric fiber;

$p$	magnitude of an applied pressure on the crack surfaces;
$Q$	electric body charge;
$Q_0$	total magnitude of an applied electric charge in a piezoelectric fiber;
$r$	radial coordinate;
$u_i$	displacements in the $i$ -direction;
$v_j$	characteristic roots of a piezoelectric material;
$w_k$	characteristic roots of a transversely isotropic elastic matrix;
$z$	vertical coordinate;
$\sigma_{ij}$	stress components;
$\varepsilon_{ij}$	strain components;
$\varepsilon_{11}^f$	dielectric constants of a piezoelectric fiber;
$\xi$	Fourier transform parameter;
$\phi$	electric potential.

## CHAPTER I

### INTRODUCTION

#### 1.1 General

Nowadays, smart materials and smart composites have found increasing applications in the fields of science and engineering such as aerospace structures, intelligent or smart structures, nondestructive testing devices, medical devices, and sensing and actuation applications. Several types of smart materials have already been developed, namely, piezoelectric materials, shape memory alloys, magnetostrictive or piezomagnetic materials, etc. Among others, piezoelectric materials have gained the most attention and widely used in practical applications. Piezoelectric materials exhibit electro-mechanical coupling phenomenon; that is, they produce an electric field when deformed under a mechanical stress (direct piezoelectric effect) and, conversely, undergo deformation when subjected to an electric field (converse piezoelectric effect). From this inherent property, piezoelectrics can be used as both actuator and sensor in a variety of applications including hydrophones, micropositioning devices, accelerometers, and structural actuators.

The low fracture strength, high stiffness, difficulty in producing complex shapes, and high density of the monolithic piezoceramic actuators all attribute to the development of the composite of piezoelectric materials. Many recent studies have examined the fabrication of piezoelectric composites and their properties (Bent et al., 1995; Nelson, 2002). Composites of piezoelectric material are classified according to their connectivity (Newnham et al., 1978). This thesis is concerned with a class of piezoelectric composites commonly known as 1-3 piezocomposites. Figure 1.1 shows a typical 1-3 piezocomposite in which the piezoceramic constituent is continuous in one direction while the matrix material is connected in all 3 orthogonal directions.



Type 1–3 connectivity piezocomposite can be designed to maximize the electromechanical coupling. The combination of fine and strong piezoceramic fibers in a polymer matrix provides load transfer mechanisms characteristic of piezoelectric fiber–reinforced composites. The soft epoxy matrix supports the brittle piezoelectric fibers and also offers more conformability of piezocomposite. Moreover, 1–3 piezocomposites exhibit higher sensitivity and lower mechanical losses than monolithic piezoelectric ceramics.

In making a 1–3 piezocomposite, several parameters can be varied: the elastic properties of the matrix material, the material properties of the piezoelectric fibers, and the volume fraction of the piezoelectric phase. Small diameter fibers can improve the performance of 1–3 piezocomposites and also offer the possibility for fiber arrangements within the composites. Three major techniques are currently used to produce fibers suitable for use in 1–3 piezocomposites: extrusion of polymer supported powders, sol–gel spinning, and the viscous suspension spinning process (VSSP). Extrusion has only been capable of producing fibers  $>100\ \mu\text{m}$  in diameter, whereas sol–gel spinning and VSSP are capable of producing fibers with diameters as small as  $10\ \mu\text{m}$ . The optimum properties of 1–3 piezocomposites are achieved for volume fraction of the piezoelectric phase around 20% (Li and Sottos, 1996; Montgomery and Richard, 1996; Rajapakse and Chen, 2008). For this volume fraction, the distance between the neighboring fibers is about four times of fiber–radius and it is reasonable to neglect the fiber–to–fiber interaction as a first approximation to study the fundamental mechanics of piezoelectric fiber–reinforced composites.

Performance and reliability of piezocomposites are governed by the interaction between the piezoelectric phase and the surrounding matrix material, which is controlled by the volume fraction of the piezoelectric phase, the material properties of the two phases and the interfacial properties. Understanding of the coupled electroelastic responses is very important to the design and reliability of devices containing piezocomposite elements. This research is an attempt to obtain a fundamental understanding of the coupled

electro–mechanical piezoelectric fiber–elastic matrix interaction in a 1–3 piezocomposite. Analytical solutions corresponding to an infinite piezoelectric fiber with a vertical body force and an infinite transversely isotropic elastic medium with a cylindrical hole are derived by using Fourier integral transforms. Based on the derived general solutions, the electro–mechanical load transfer and interfacial fracture in piezoelectric fiber–reinforced composites are formulated. A computer program is developed to analyze the load transfer and the interfacial fracture problems, and to investigate the influence of various parameters on the electroelastic responses in piezocomposites.

## 1.2 Objectives of Present Study

The objectives of this research are given as follows.

1) To derive the analytical general solutions for an infinite piezoelectric fiber with body forces and electric charge, and an infinite transversely isotropic elastic media with a cylindrical hole. These general solutions are necessary for the analysis of the load transfer mechanism and the interface dislocation in a piezoelectric fiber–reinforced composite.

2) To conduct a comprehensive study on the electro–mechanical load transfer mechanism of a piezoelectric fiber–reinforced composite and investigate the effect of various parameters, e.g. fiber and matrix material properties, electrical boundary conditions, interface conditions etc., on the electroelastic responses of a piezocomposite.

3) To conduct a theoretical study on the fracture mechanics of a piezoelectric fiber–reinforced composite with a cylindrical interface crack based on the displacement discontinuity method and the fundamental solutions of interface dislocation.

### 1.3 Scopes of Present Study

This thesis is concerned with the theoretical study of the electroelastic responses in piezocomposites. The case of a long cylindrical piezoelectric fiber embedded in an infinite transversely isotropic elastic matrix is considered. Both fiber and matrix are assumed to be transversely isotropic with the principal material directions parallel to the fiber direction. The electroelastic load transfer and interfacial fracture of piezocomposites are studied in details. For the load transfer problem, the imperfect fiber–matrix interface is represented by a spring–factor model. Except along the crack surfaces, the fiber–matrix is assumed to be perfectly bonded in the analysis of interfacial fracture. Only axisymmetric loading and geometry are considered in this study.

### 1.4 Basic Assumptions

The electro–mechanical interaction between a piezoelectric fiber and an elastic matrix considered in this study is based on the following assumptions:

1. A piezoelectric fiber is homogeneous, transversely isotropic and governed by linear piezoelectricity theory.
2. The fiber–to–fiber effect in a 1–3 piezocomposite is negligible.
3. A matrix is a transversely isotropic elastic material.
4. The bond between the fiber and the matrix is assumed to be perfect except along the crack surfaces. The imperfect interface considered in the study of electroelastic load transfer mechanism is represented by a spring–factor model.

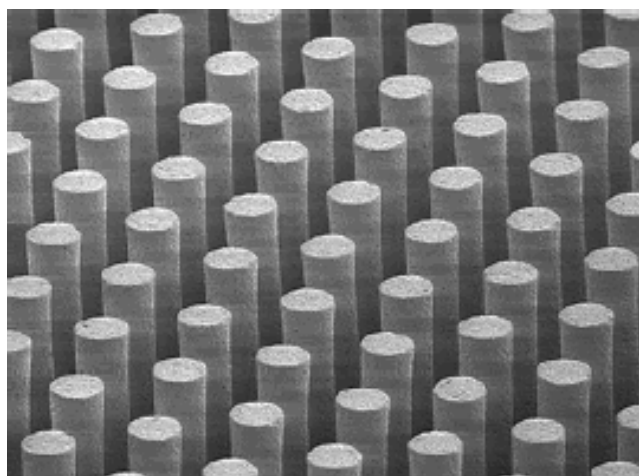


**Figure 1.1** A 1–3 piezocomposite.

## CHAPTER II

### LITERATURE REVIEWS

#### 2.1 General

Piezoelectric materials have been extensively used as transducers and sensors due to their intrinsic direct and converse piezoelectric effects that take place between electric fields and mechanical deformation, and they are playing a key role as active components in many branches of engineering and technology science (Rao & Sunar, 1994). Early studies by Mindlin (1974), Chen (1980), Deeg (1980) and others have addressed some fundamental problems related to mechanics of piezoelectric materials. The theoretical foundation and electroelastic governing equations of piezoelectric materials are presented by Parton and Kudryavtsev (1988). Thereafter, many researchers provided the theoretical study and analytical solution for plane problem of piezoelectric materials, e.g. Sosa (1991), Rajapakse (1997), Xu and Rajapakse (2000a, 2001). Piezoceramic cylinders, which are the common forms of structural elements used in sensor and actuator applications, have also been studied by Rajapakse and Zhou (1997) for the case of infinite piezoelectric solid cylinder subjected to a radial ring load and a ring electric charge; and by Rajapakse et al. (2005) and Senjuntichai et al. (2008) for piezoelectric annular and solid finite cylinder respectively.

#### 2.2 Fiber–Matrix Interaction

Performance and reliability of composite materials are governed by several parameters, such as the volume ratio, the interfacial properties, and the properties of the fiber and the surrounding matrix material. The study of the fiber–matrix interaction is therefore the key issue for better design and development of reliable composite materials in advanced engineering

applications. The study of fiber–matrix interaction in the conventional composite materials has a rich history. Muki and Sternberg (1969) examined the three–dimensional interaction of a single infinitely long cylindrical fiber in an isotropic matrix by studying the diffusion of an axial load from the fiber into the matrix. They gave an exact analytical solution based on the theory of elasticity for a circular fiber and proposed an approximate solution scheme for a fiber with an arbitrary cross section. Thereafter, the load transfer mechanics between fiber and matrix have been studied by several researchers, namely, Pak and Gobert (1993), Slaughter and Sanders (1991), etc. In the context of civil engineering, this problem is mathematically identical to load transfer from a pile into the surrounding earth (Niumpradit & Karasudhi, 1981; Selvadurai & Rajapakse, 1990; Senjuntichai et al., 2007).

Most of the works presented in the literature on the mechanics of composite materials have concerned with the classical situation where the displacements and surface tractions are continuous across the fiber–matrix boundary, the so–called perfect bonding condition. It is well known, however, that load transfer mechanism depends significantly on the properties of the interphasial layer which leads to an imperfect bonding between the fiber and the matrix. The imperfect interface is encountered in the composite materials for various reasons, for example, thin interphase of adhesion coating, chemical action during manufacturing process, or interfacial damage between the fiber and matrix.

The interphasial layer between fibers and matrix has very complicated microstructure and has different material properties from both the fiber and the matrix. Generally, there are unlikely to have detailed information about the thickness or the material properties of the interphase. Therefore, assumptions are employed in the modeling, such as the widely used spring–factor model which assumes the displacement jump across the interface to be proportional to the corresponding interfacial stresses (Mal and Bose, 1975; Hammamia et al., 2006). The spring–factor model for imperfect interface were employed by

Nairn and Liu (1996) and Lenci and Menditto (2000) among others, in the analysis of elastic fiber–reinforced composites.

A review of literature indicates that the studies on fiber–matrix interaction in piezocomposites are very limited. Rajapakse (1996) examined the electroelastic field of a long elastic cylinder with a piezoelectric core subjected to an external radial pressure band. Liu et al. (2003) and Gu et al. (2006) studied the interaction between the stress and electric fields for a single piezoelectric fiber pullout from an elastic matrix under mechanical and electric loads. Their analysis are simplified by ignoring the radial variations of the stresses and strains in both the fiber and matrix and the electric field in the fiber. A rigorous study of the fiber–matrix interaction and electro–mechanical load transfer in 1–3 piezocomposites with the consideration of the imperfect interface is currently not available.

### 2.3 Cracks in Piezocomposites

Naturally, fiber–reinforced composites consist of several constituents of different geometry and properties, joined along the interfaces. These factors usually contribute to fracture problems in the composites. The common forms of a fracture problem in fiber–reinforced composites are voids and crackings near or on the fiber–matrix interface introduced during fabrications and under service loading. A majority of studies considered the problem of cracks with plane surfaces, and only a few were concerned with curved surfaces, which are mathematically more difficult. When crack–like defects on the interface are distributing in the circumferential direction around a fiber, a cylindrical crack must be considered in the fracture modeling. Demir et al. (1992) analyzed the pressurized cylindrical crack in an infinite homogeneous isotropic elastic medium and obtained the stress and displacement field around the crack based on the fundamental solutions of the Somigliana ring dislocation. Erdogan and Özbek (1969) considered an elastic fiber reinforced composite with a cylindrical interface crack using a singular integral equation method.

The counterpart problems in transversely isotropic elasticity were also studied by Kasano et al. (1984).

The subject of cracks in piezoelectric materials, for various failure modes, has received considerable attention in the last decade. Fracture mechanics experiments were performed by several researchers for three-point bending, compact tension and double cantilever beam specimens under mechanical and/or electrical loading (Park and Sun, 1995; Heyer et al., 1998). Several analytical methods, such as integral transformation, singular integral equations, Lekhnitskii's approach (Lekhnitskii, 1981) and Stroh's formulation (Stroh, 1958 & 1962), have been adopted for linear elastic fracture mechanics (LEFM) analysis of piezoelectric materials (Deeg, 1980; Sosa and Pak, 1990; Suo et al., 1992; Sosa, 1992; Pak, 1992; Park and Sun, 1995; Xu and Rajapakse, 1999 & 2000a).

The study on fracture mechanics for piezoelectric solids based on the analytical approaches are mostly restricted to simple geometries and loading conditions. Boundary element-based methods for fracture analysis are versatile tools that can be used for the analysis of complex fracture mechanics problems (Cruise, 1988). Pan (1999) and Rajapakse and Xu (2001) reported a single-domain BEM formulation for fracture mechanics analysis in cracked 2D piezoelectric solids. The displacement discontinuity method (DDM), which is an indirect boundary element method proposed by Crouch and Starfield (1983), can be extended to consider fracture mechanics of piezoelectric solids. The DDM has been demonstrated to be successful for two and three dimensional elastostatic problems (Crouch & Starfield, 1983; Sladek & Sladek, 1982).

The field intensity factor is an important concept in fracture mechanics. Based on an impermeable crack model, Sosa (1992) and Suo et al. (1992) introduced an electric intensity factor for cracks in a piezoelectric material in addition to the well known stress intensity factors. For cracks in a homogeneous piezoelectric material, the mechanical stresses and the electric



displacements show a classical square root singularity at the crack tip. However, cracks at the interface of piezocomposites may contain singularity beside the classical  $1/2$  singularity. Based on the extended Stroh formalism, Suo et al. (1992) discussed the singularities of interfacial cracks in bonded anisotropic piezoelectric media. Ou (2003) and Ou and Chen (2004) studied the crack-tip singularity of interfacial cracks in transversely isotropic piezoelectric bimetals and presented the numerical evaluations of the singularity index for composites of commercially available piezoelectric ceramics. A comprehensive treatment of singularities in multi-material piezoelectric wedges and junctions was also presented by Xu and Rajapakse [40] by extending Lekhnitskii's formalism for elastic anisotropic solids.

## CHAPTER III

### BASIC EQUATIONS AND GENERAL SOLUTIONS

In this chapter, the basic equations for piezoelectricity and the governing equations for torsionless three-dimensional axisymmetric deformations of a transversely isotropic piezoelectric material expressed in terms of displacements and electric potential are presented. The general solutions for axisymmetric deformations of piezoelectric and elastic materials are then derived by solving the governing equations through the application of Fourier integral transforms. These general solutions will be used to analyze the load transfer problem of fiber-reinforced composite and to derive the fundamental solutions of interface dislocations in the analysis of interfacial crack in piezoelectric fiber-reinforced composites in the subsequent chapters.

#### 3.1 Basic Equations

Consider a smart composite consisting of an infinite cylindrical piezoelectric fiber of radius “ $a$ ” embedded in an unbounded elastic matrix. Both piezoelectric fiber and elastic matrix are transversely isotropic. A cylindrical polar coordinate system  $(r, \theta, z)$  is used with the  $z$ -axis parallel to the axis of symmetry of both the fiber and the matrix (Figure 3.1).

The constitutive equations for a piezoelectric material that are transversely isotropic or poled along the  $z$ -axis can be expressed as (Parton & Kudryavtsev, 1988),

$$\sigma_{rr} = c_{11}^f \varepsilon_{rr} + c_{12}^f \varepsilon_{\theta\theta} + c_{13}^f \varepsilon_{zz} - e_{31}^f E_z \quad (3.1a)$$

$$\sigma_{\theta\theta} = c_{12}^f \varepsilon_{rr} + c_{11}^f \varepsilon_{\theta\theta} + c_{13}^f \varepsilon_{zz} - e_{31}^f E_z \quad (3.1b)$$

$$\sigma_{zz} = c_{13}^f \varepsilon_{rr} + c_{13}^f \varepsilon_{\theta\theta} + c_{33}^f \varepsilon_{zz} - e_{33}^f E_z \quad (3.1c)$$

$$\sigma_{rz} = 2c_{44}^f \varepsilon_{rz} - e_{15}^f E_r \quad (3.1d)$$

$$D_z = e_{31}^f \varepsilon_{rr} + e_{31}^f \varepsilon_{\theta\theta} + e_{33}^f \varepsilon_{zz} + \varepsilon_{33}^f E_z \quad (3.1e)$$

$$D_r = 2e_{15}^f \varepsilon_{rz} + \varepsilon_{11}^f E_r \quad (3.1f)$$

where  $\sigma_{rr}$ ,  $\sigma_{\theta\theta}$ ,  $\sigma_{zz}$  and  $\sigma_{rz}$  denote the stress components;  $\varepsilon_{rr}$ ,  $\varepsilon_{\theta\theta}$ ,  $\varepsilon_{zz}$  and  $\varepsilon_{rz}$  denote the strain components;  $D_r$  and  $D_z$  denote the electric displacement vectors in the  $r$ - and  $z$ -directions respectively;  $E_r$  and  $E_z$  denote the electric fields in the  $r$ - and  $z$ -directions respectively;  $c_{11}^f$ ,  $c_{12}^f$ ,  $c_{13}^f$ ,  $c_{33}^f$  and  $c_{44}^f$  denote the elastic constants under zero or constant electric field;  $e_{31}^f$ ,  $e_{33}^f$  and  $e_{15}^f$  denote the piezoelectric constants; and  $\varepsilon_{11}^f$  and  $\varepsilon_{33}^f$  denote the dielectric constants under zero or constant strain.

It is noted that the constitutive equations for a transversely isotropic matrix material can be obtained from equations (3.1a)–(3.1d) by setting  $e_{ij}^f = \varepsilon_{ij}^f \equiv 0$  and replacing  $c_{ij}^f$  by  $c_{ij}^m$ . The strain–displacement relations are given by

$$\varepsilon_{rr} = \frac{\partial u_r}{\partial r}; \quad \varepsilon_{\theta\theta} = \frac{u_r}{r}; \quad \varepsilon_{zz} = \frac{\partial u_z}{\partial z}; \quad \varepsilon_{zr} = \frac{1}{2} \left( \frac{\partial u_r}{\partial z} + \frac{\partial u_z}{\partial r} \right) \quad (3.2)$$

where  $u_r$  and  $u_z$  denote the displacements in the  $r$ - and  $z$ -directions respectively.

The field equations of a piezoelectric material undergoing axisymmetric deformations about the  $z$ -axis can be expressed as

$$\frac{\partial \sigma_{rr}}{\partial r} + \frac{\partial \sigma_{rz}}{\partial z} + \frac{\sigma_{rr} - \sigma_{\theta\theta}}{r} + F_r = 0 \quad (3.3a)$$

$$\frac{\partial \sigma_{rz}}{\partial r} + \frac{\partial \sigma_{zz}}{\partial z} + \frac{\sigma_{rz}}{r} + F_z = 0 \quad (3.3b)$$

$$\frac{\partial D_r}{\partial r} + \frac{\partial D_z}{\partial z} + \frac{D_r}{r} - Q = 0 \quad (3.3c)$$

where  $F_r$  and  $F_z$  denote the body forces in the  $r$ - and  $z$ -directions respectively, and  $Q$  denotes the electric body charge.

The electric field  $E_i$  ( $i = r, z$ ) and the electric potential  $\phi(r, z)$  are related by

$$E_r = -\frac{\partial \phi}{\partial r}; \quad E_z = -\frac{\partial \phi}{\partial z} \quad (3.4)$$

Substitution of equations (3.1), (3.2) and (3.4) in the field equations (3.3) results in the following governing equations in terms of the displacement  $u_r$  and  $u_z$  in the  $r$ - and  $z$ -directions and the electric potential  $\phi(r, z)$  (Rajapakse and Zhou, 1997):

$$c_{11}^f \left( \frac{\partial^2 u_r}{\partial r^2} + \frac{1}{r} \frac{\partial u_r}{\partial r} - \frac{1}{r^2} u_r \right) + c_{44}^f \frac{\partial^2 u_r}{\partial z^2} + (c_{13}^f + c_{44}^f) \frac{\partial^2 u_z}{\partial r \partial z} + (e_{31}^f + e_{15}^f) \frac{\partial^2 \phi}{\partial r \partial z} + F_r = 0 \quad (3.5a)$$

$$c_{44}^f \left( \frac{\partial^2 u_z}{\partial r^2} + \frac{1}{r} \frac{\partial u_z}{\partial r} \right) + c_{33}^f \frac{\partial^2 u_z}{\partial z^2} + (c_{13}^f + c_{44}^f) \left( \frac{\partial^2 u_r}{\partial r \partial z} + \frac{1}{r} \frac{\partial u_r}{\partial z} \right) + e_{15}^f \left( \frac{\partial^2 \phi}{\partial r^2} + \frac{1}{r} \frac{\partial \phi}{\partial r} \right) + e_{33}^f \frac{\partial^2 \phi}{\partial z^2} + F_z = 0 \quad (3.5b)$$

$$e_{15}^f \left( \frac{\partial^2 u_z}{\partial r^2} + \frac{1}{r} \frac{\partial u_z}{\partial r} \right) + e_{33}^f \frac{\partial^2 u_z}{\partial z^2} + (e_{31}^f + e_{15}^f) \left( \frac{\partial^2 u_r}{\partial r \partial z} + \frac{1}{r} \frac{\partial u_r}{\partial z} \right) - \epsilon_{11}^f \left( \frac{\partial^2 \phi}{\partial r^2} + \frac{1}{r} \frac{\partial \phi}{\partial r} \right) - \epsilon_{33}^f \frac{\partial^2 \phi}{\partial z^2} - Q = 0 \quad (3.5c)$$

### 3.2 General Solutions of Piezoelectric Materials

A generalized displacement potential function  $\psi(r, z)$  is introduced by relating it to the displacements  $u_r$  and  $u_z$  and the electric potential  $\phi$  in the following manner (Wang and Zheng, 1995):

$$u_r = \frac{\partial \psi}{\partial r}; \quad u_z = k_1 \frac{\partial \psi}{\partial z}; \quad \phi = k_2 \frac{\partial \psi}{\partial z} \quad (3.6)$$

where  $k_1$  and  $k_2$  are unknown constants to be determined.

The substitution of equation (3.6) into equations (3.5) results in the following governing equations to determine  $\psi$ ,  $k_1$  and  $k_2$ .

$$\frac{\partial}{\partial r} \left[ c_{11}^f \left( \frac{\partial^2 \psi}{\partial r^2} + \frac{1}{r} \frac{\partial \psi}{\partial r} \right) + \{ c_{44}^f + (c_{13}^f + c_{44}^f)k_1 + (e_{31}^f + e_{15}^f)k_2 \} \frac{\partial^2 \psi}{\partial z^2} \right] + F_r = 0 \quad (3.7a)$$

$$\frac{\partial}{\partial z} \left[ (c_{13}^f + c_{44}^f + c_{44}^f k_1 + e_{15}^f k_2) \left( \frac{\partial^2 \psi}{\partial r^2} + \frac{1}{r} \frac{\partial \psi}{\partial r} \right) + (c_{33}^f k_1 + e_{33}^f k_2) \frac{\partial^2 \psi}{\partial z^2} \right] + F_z = 0 \quad (3.7b)$$

$$\frac{\partial}{\partial z} \left[ (e_{31}^f + e_{15}^f + e_{15}^f k_1 - \varepsilon_{11}^f k_2) \left( \frac{\partial^2 \psi}{\partial r^2} + \frac{1}{r} \frac{\partial \psi}{\partial r} \right) + (e_{33}^f k_1 - \varepsilon_{33}^f k_2) \frac{\partial^2 \psi}{\partial z^2} \right] - Q = 0 \quad (3.7c)$$

The solution for the potential function  $\psi(r, z)$  composes of the homogeneous solution, denoted by  $\psi^h(r, z)$ , and the particular solution, denoted by  $\psi^p(r, z)$  such that,

$$\psi(r, z) = \psi^h(r, z) + \psi^p(r, z) \quad (3.8)$$

### 3.2.1 Homogeneous Solution

The homogeneous solution of the potential function,  $\psi^h(r, z)$ , is derived from equations (3.7a)–(3.7c) by setting  $F_r = F_z = Q = 0$  and applying Fourier integral transforms with respect to  $z$ . The Fourier integral transform of a function  $f(r, z)$  with respect to  $z$  and its inverse are defined by (Sneddon, 1970)

$$\bar{f}(r, \xi) = \frac{1}{\sqrt{2\pi}} \int_{-\infty}^{\infty} f(r, z) e^{i\xi z} dz \quad (3.9a)$$

$$f(r, z) = \frac{1}{\sqrt{2\pi}} \int_{-\infty}^{\infty} \bar{f}(r, \xi) e^{-i\xi z} d\xi \quad (3.9b)$$

where  $\xi$  denotes the Fourier transform parameter.

Applying the Fourier integral transforms to equations (3.7a)–(3.7c) with  $F_r = F_z = Q = 0$ , the following homogeneous solution can be obtained,

$$\bar{\psi}^h(r, \xi) = \sum_{j=1}^3 \left[ I_0(\xi_j r) A_j(\xi) + K_0(\xi_j r) B_j(\xi) \right] \quad (3.10a)$$

where

$$\xi_j = |\xi| \sqrt{v_j}; \quad j = 1, 2, 3 \quad (3.10b)$$

and  $\bar{\psi}^h$  ( $j=1,2,3$ ) is the Fourier transform of the homogeneous solution of the potential function;  $v_j$  ( $j = 1,2,3$ ) is a set of roots of the characteristic equation corresponding to equations (3.7) and defined in the Appendix A;  $A_j(\xi)$  and  $B_j(\xi)$  ( $j = 1, 2, 3$ ) are arbitrary functions to be determined from the boundary and continuity conditions;  $I_n$  and  $K_n$  denote the modified Bessel functions of the first and the second kinds of order  $n$  respectively (Watson, 1962).

Let  $k_{1j}^h$  and  $k_{2j}^h$  denote the constants  $k_1$  and  $k_2$  of the homogeneous solution corresponding to the root  $v_j$ . It can be shown that

$$k_{1j}^h = \frac{c_{11}^f v_j - c_{44}^f - (e_{15}^f + e_{31}^f) k_{2j}^h}{c_{13}^f + c_{44}^f} \quad (3.11a)$$

$$k_{2j}^h = \frac{(c_{11}^f v_j - c_{44}^f)(c_{33}^f - c_{44}^f v_j) - (c_{13}^f + c_{44}^f)^2 v_j}{(e_{15}^f + e_{31}^f)(c_{33}^f - c_{44}^f v_j) - (c_{13}^f + c_{44}^f)(e_{33}^f - e_{15}^f v_j)} \quad (3.11b)$$

Note that the homogenous general solution given by equation (3.10) corresponds to an infinite annular piezoelectric cylinder. The solution for a solid piezoelectric fiber of finite radius can be obtained from equation (3.10a) by setting  $B_j = 0$ .

### 3.2.2 Particular Solution

The particular solutions of the equations (3.7) under a non-zero axial body force and a body charge are derived in this section. This particular solution does not exist in the literature. First, consider the case of a vertical body force  $F_z(z)$  in the absence of a radial body force  $F_r$  and a body charge  $Q$ . To satisfy equation (3.7) for any arbitrary  $r$ -value, the particular solution  $\psi^p$  must be independent of  $r$ . Consequently, the terms  $[(\partial^2 \psi^p / \partial r^2) + (1/r)(\partial \psi^p / \partial r)]$  appeared in equation (3.7) are vanished. The constants  $k_1$  and  $k_2$  of the particular solution corresponding to a vertical body force are denoted by  $k_1^{pz}$  and  $k_2^{pz}$ . These constants can be determined from equations (3.7a) and (3.7c) with  $F_r = Q = 0$  as

$$k_1^{pz} = \frac{-c_{44}^f \varepsilon_{33}^f}{(e_{31}^f + e_{15}^f) e_{33}^f + (c_{13}^f + c_{44}^f) \varepsilon_{33}^f} \quad (3.12a)$$

$$k_2^{pz} = \frac{e_{33}^f}{\varepsilon_{33}^f} k_1^{pz} \quad (3.12b)$$

Applying Fourier transforms to equation (3.7b), the following solution for the Fourier transform of the particular solution of the potential function can be obtained.

$$\bar{\psi}^{pz}(\xi) = \frac{i\bar{F}_z(\xi)}{\xi^3 (c_{33}^f k_1^{pz} + e_{33}^f k_2^{pz})} \quad (3.13)$$

where  $\bar{F}_z(\xi)$  denotes the Fourier transform of the vertical body force.

Next consider the case of an electric body charge with  $F_r = F_z = 0$ . Similar to the case of a vertical body force, the expressions for  $k_1^{pq}$  and  $k_2^{pq}$  for the case of an electric body charge can be determined from equations (3.7a) and (3.7b) as

$$k_1^{pq} = \frac{c_{44}^f e_{33}^f}{(e_{31}^f + e_{15}^f) c_{33}^f - (c_{13}^f + c_{44}^f) e_{33}^f} \quad (3.14a)$$

$$k_2^{pq} = -\frac{c_{33}^f}{e_{33}^f} k_1^{pq} \quad (3.14b)$$

The Fourier transform of the particular solution  $\bar{\psi}^{pq}$  corresponding to the case of an electric charge  $Q(z)$  is obtained from equation (3.7c) as

$$\bar{\psi}^{pq}(\xi) = \frac{-i\bar{Q}(\xi)}{\xi^3 (e_{33}^f k_1^{pq} - \varepsilon_{33}^f k_2^{pq})} \quad (3.15)$$

where  $\bar{Q}(\xi)$  denotes the Fourier transform of the body charge.

### 3.2.3 Complete General Solutions

By using the homogeneous and particular solutions presented in the foregoing subsections, the complete general solutions for the Fourier transforms of the electroelastic fields of a piezoelectric fiber can be expressed as

$$\bar{u}_r(r, \xi) = \sum_{j=1}^3 \xi_j I_1(\xi_j r) A_j(\xi) \quad (3.16a)$$

$$\bar{u}_z(r, \xi) = -i\xi \left[ \sum_{j=1}^3 k_{1j}^h I_0(\xi_j r) A_j(\xi) + k_1^{pz} \bar{\psi}^{pz}(\xi) + k_1^{pq} \bar{\psi}^{pq}(\xi) \right] \quad (3.16b)$$

$$\bar{\phi}(r, \xi) = -i\xi \left[ \sum_{j=1}^3 k_{2j}^h I_0(\xi_j r) A_j(\xi) + k_2^{pz} \bar{\psi}^{pz}(\xi) + k_2^{pq} \bar{\psi}^{pq}(\xi) \right] \quad (3.16c)$$

$$\begin{aligned} \bar{\sigma}_{rr}(r, \xi) = \sum_{j=1}^3 \left\{ |\xi|^2 \left[ c_{11}^f v_j - c_{13}^f k_{1j}^h - e_{31}^f k_{2j}^h \right] I_0(\xi_j r) + (c_{12}^f - c_{11}^f) \xi_j r^{-1} I_1(\xi_j r) \right\} A_j(\xi) \\ - \xi^2 \left[ (c_{13}^f k_1^{pz} + e_{31}^f k_2^{pz}) \bar{\psi}^{pz}(\xi) + (c_{13}^f k_1^{pq} + e_{31}^f k_2^{pq}) \bar{\psi}^{pq}(\xi) \right] \end{aligned} \quad (3.16d)$$

$$\begin{aligned} \bar{\sigma}_{\theta\theta}(r, \xi) = \sum_{j=1}^3 \left\{ |\xi|^2 \left[ c_{12}^f v_j - c_{13}^f k_{1j}^h - e_{31}^f k_{2j}^h \right] I_0(\xi_j r) + (c_{11}^f - c_{12}^f) \xi_j r^{-1} I_1(\xi_j r) \right\} A_j(\xi) \\ - \xi^2 \left[ (c_{13}^f k_1^{pz} + e_{31}^f k_2^{pz}) \bar{\psi}^{pz}(\xi) + (c_{13}^f k_1^{pq} + e_{31}^f k_2^{pq}) \bar{\psi}^{pq}(\xi) \right] \end{aligned} \quad (3.16e)$$

$$\begin{aligned} \bar{\sigma}_{zz}(r, \xi) = \sum_{j=1}^3 |\xi|^2 \left[ c_{33}^f v_j - c_{33}^f k_{1j}^h - e_{33}^f k_{2j}^h \right] I_0(\xi_j r) A_j(\xi) \\ - \xi^2 \left[ (c_{33}^f k_1^{pz} + e_{33}^f k_2^{pz}) \bar{\psi}^{pz}(\xi) + (c_{33}^f k_1^{pq} + e_{33}^f k_2^{pq}) \bar{\psi}^{pq}(\xi) \right] \end{aligned} \quad (3.16f)$$

$$\bar{\sigma}_{rz}(r, \xi) = -i\xi \sum_{j=1}^3 \xi_j \left[ c_{44}^f (1 + k_{1j}^h) - e_{15}^f k_{2j}^h \right] I_1(\xi_j r) A_j(\xi) \quad (3.16g)$$

$$\bar{D}_r(r, \xi) = -i\xi \sum_{j=1}^3 \xi_j \left[ e_{15}^f (1 + k_{1j}^h) - \varepsilon_{11}^f k_{2j}^h \right] I_1(\xi_j r) A_j(\xi) \quad (3.16h)$$

$$\begin{aligned} \bar{D}_z(r, \xi) = \sum_{j=1}^3 |\xi|^2 \left[ e_{31}^f v_j - e_{33}^f k_{1j}^h + \varepsilon_{33}^f k_{2j}^h \right] I_0(\xi_j r) A_j(\xi) \\ - \xi^2 \left[ (e_{33}^f k_1^{pz} - \varepsilon_{33}^f k_2^{pz}) \bar{\psi}^{pz}(\xi) + (e_{33}^f k_1^{pq} - \varepsilon_{33}^f k_2^{pq}) \bar{\psi}^{pq}(\xi) \right] \end{aligned} \quad (3.16i)$$

The three arbitrary functions  $A_j$  ( $j = 1, 2, 3$ ) appearing in equations (3.16) can be determined from the three boundary conditions (two mechanical and one electric conditions) associated with the outer surface of the piezoelectric fiber.

### 3.3 General Solutions of Transversely Isotropic Elastic Materials

Let consider the surrounding elastic matrix in a piezocomposite shown in Figure 3.1. The matrix is transversely isotropic and free from any body force. The general solution can be derived by following a similar procedure given in Section



3.2 for the piezoelectric case, and setting  $e_{ij}^f = \varepsilon_{ij}^f \equiv 0$  and replacing  $c_{ij}^f$  by  $c_{ij}^m$ . It can be shown that the analytical general solutions for the Fourier transforms of displacements and stresses for a transversely isotropic elastic matrix with a cylindrical hole are given by

$$\bar{u}_r(r, \xi) = \sum_{k=1}^2 \xi_k K_1(\xi_k r) C_k(\xi) \quad (3.17a)$$

$$\bar{u}_z(r, \xi) = -i\xi \sum_{k=1}^2 n_k K_0(\xi_k r) C_k(\xi) \quad (3.17b)$$

$$\begin{aligned} \bar{\sigma}_{rr}(r, \xi) = \sum_{k=1}^2 \left\{ |\xi|^2 [c_{11}^m w_k - c_{13}^m n_k] K_0(\xi_k r) \right. \\ \left. - [c_{12}^m - c_{11}^m] \xi_k r^{-1} K_1(\xi_k r) \right\} C_k(\xi) \end{aligned} \quad (3.17c)$$

$$\begin{aligned} \bar{\sigma}_{\theta\theta}(r, \xi) = \sum_{k=1}^2 \left\{ |\xi|^2 [c_{12}^m w_k - c_{13}^m n_k] K_0(\xi_k r) \right. \\ \left. - [c_{11}^m - c_{12}^m] \xi_k r^{-1} K_1(\xi_k r) \right\} C_k(\xi) \end{aligned} \quad (3.17d)$$

$$\bar{\sigma}_{zz}(r, \xi) = \sum_{k=1}^2 |\xi|^2 [c_{13}^m w_k - c_{33}^m n_k] K_0(\xi_k r) C_k(\xi) \quad (3.17e)$$

$$\bar{\sigma}_{rz}(r, \xi) = i\xi \sum_{k=1}^2 \xi_k c_{44}^m [1 + n_k] K_1(\xi_k r) C_k(\xi) \quad (3.17f)$$

where  $c_{ij}^m$  denotes the elastic constants of the matrix material;  $C_k(\xi)$  ( $k = 1, 2$ ) are the arbitrary functions to be determined from the boundary and continuity conditions; and

$$\xi_k = |\xi| \sqrt{w_k}; \quad n_k = \frac{c_{11}^m w_k - c_{44}^m}{c_{13}^m + c_{44}^m}; \quad k = 1, 2 \quad (3.18)$$

In addition,  $w_k$  ( $k = 1, 2$ ) are the roots of the following equation.

$$c_{11}^m c_{44}^m w_k^2 + \left[ (c_{13}^m)^2 + 2c_{13}^m c_{44}^m - c_{11}^m c_{33}^m \right] w_k + c_{33}^m c_{44}^m = 0 \quad (3.19)$$

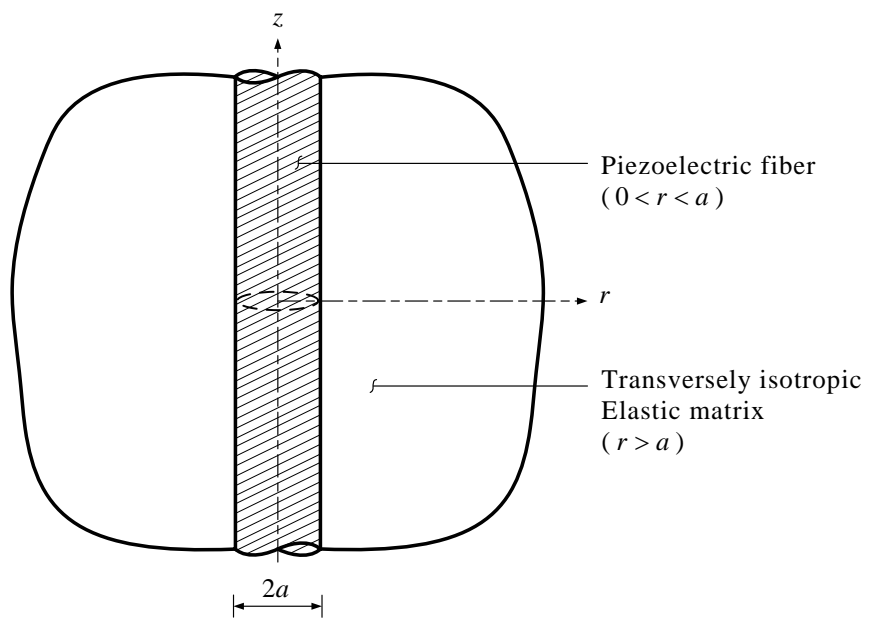


Figure 3.1 A piezoelectric fiber-reinforced composite.

## CHAPTER IV

### ELECTRO–MECHANICAL LOAD TRANSFER IN PIEZOCOMPOSITES

In this chapter, the electro–mechanical interaction between a fiber and a matrix material in a piezocomposite due to an axial load and electric charge applied to the fiber as shown in Figure 4.1 is considered. The fiber–matrix interface is considered to be mechanically imperfect and is represented by a spring–factor model. The interface is either electrically open– or short–circuited. The general solutions presented in the preceding Chapter are used to formulate the load transfer boundary–value problem. Numerical results for the axial force, electric field, displacements and interfacial stresses are presented to demonstrate electro–mechanical interaction in a fiber–matrix system. Finally, the influence of the interface stiffness on the electromechanical load diffusion in a piezoelectric fiber–reinforced composite is investigated.

#### 4.1 Problem Formulation

The general solutions derived in the preceding chapter are used in the analysis of the fundamental electro–mechanical fiber–matrix interaction problem shown in Figure 4.1. The fiber–matrix interface is assumed to be either electrically open– or short–circuited and mechanically imperfect. The general solution of the fiber and matrix are given by equations (3.16) and (3.17) respectively. These equations involve five arbitrary functions,  $A_1$ ,  $A_2$ ,  $A_3$ ,  $C_1$  and  $C_2$  which can be determined from the continuity conditions along the fiber–matrix interface for a specified body force  $F_z(z)$  and/or electric charge  $Q(z)$ . In this study, the fundamental solutions involving an axial force and an electric charge applied uniformly over the fiber cross section at  $z=0$  (Figure 4.1) are considered. The total magnitude of the applied axial force and electric charge are  $P_0$  and  $Q_0$  respectively. The corresponding body force functions  $F_z(z)$  and  $Q(z)$  can be expressed as

$$F_z(z) = -P_0 \delta(z)/(\pi a^2) \quad (4.1a)$$

$$Q(z) = -Q_0 \delta(z)/(\pi a^2) \quad (4.1b)$$

The stress continuity conditions and electrically impermeable condition (open-circuited) along the fiber–matrix interface ( $r = a$ ) can be expressed as

$$\sigma_{rr}^f(a, z) = \sigma_{rr}^m(a, z) \quad (4.2a)$$

$$\sigma_{rz}^f(a, z) = \sigma_{rz}^m(a, z) \quad (4.2b)$$

$$D_r^f(a, z) = 0 \quad (4.2c)$$

in which the superscript  $f$  and  $m$  are used to identify the quantities corresponding to the piezoelectric fiber ( $0 \leq r \leq a$ ) and the elastic matrix ( $a \leq r < \infty$ ) respectively.

Alternately, the electric boundary condition in equation (4.2) can be replaced by  $\phi^f(a, z) = 0$  which implies short-circuited condition. The two conditions represent the extreme electric boundary conditions at the fiber–matrix interface.

In the present study, the mechanically imperfect fiber–matrix interface is represented by a spring–factor model, which assumes that sufficient cohesion exists on the interface to prevent separation in the radial direction, and relates the vertical displacement jump along the interface and the interface shear stress through a spring–factor parameter as follows

$$u_r^f(a, z) = u_r^m(a, z) \quad (4.3a)$$

$$k_s [u_z^m(a, z) - u_z^f(a, z)] = \sigma_{rz}^f(a, z) \quad (4.3b)$$

where  $k_s$  denotes the spring–factor parameter.

For a perfectly bonded interface,  $k_s \rightarrow \infty$  and  $u_z^f(a, z) = u_z^m(a, z)$ . Equations (4.1)–(4.3) can be easily expressed in the Fourier transform domain and the substitution of general solutions given by equations (3.16) and (3.17) in

equations (4.2) and (4.3) results in a linear algebraic simultaneous equation system to determine the arbitrary functions  $A_1$ ,  $A_2$ ,  $A_3$ ,  $C_1$  and  $C_2$ . Once the arbitrary functions are determined, the full electroelastic field of the system shown in Figure 4.1 can be determined.

Application of the inverse Fourier integral transforms to equation (3.16f) results in the following solution for normal stress  $\sigma_{zz}^f(r, z)$  in the piezoelectric fiber.

$$\sigma_{zz}^f(r, z) = \frac{1}{\sqrt{2\pi}} \int_{-\infty}^{\infty} \left\{ |\xi|^2 \left[ c_{13}^f v_j - c_{33}^f k_{1j}^h - e_{33}^f k_{2j}^h \right] I_0(\xi_j r) A_j(\xi) - \xi^2 \left[ (c_{33}^f k_1^{pz} + e_{33}^f k_2^{pz}) \bar{\psi}^{pz}(\xi) + (c_{33}^f k_1^{pq} + e_{33}^f k_2^{pq}) \bar{\psi}^{pq}(\xi) \right] \right\} e^{-i\xi z} d\xi \quad (4.4)$$

The resultant axial force  $P(z)$  in the piezoelectric fiber at a given cross section can be determined from

$$P(z) = 2\pi \int_0^a \sigma_{zz}^f(r, z) r dr; \quad -\infty < z < \infty \quad (4.5)$$

Substitution of the solution of  $\sigma_{zz}^f(r, z)$  into equation (4.5) and use of the following identity (Watson, 1972)

$$\int r I_0(\xi r) dr = \frac{r I_1(\xi r)}{\xi} \quad (4.6)$$

yields

$$P(z) = \sqrt{2\pi} a \int_{-\infty}^{\infty} \left\{ \sum_{j=1}^3 \frac{|\xi|}{\sqrt{v_j}} (c_{13}^f v_j - c_{33}^f k_{1j}^h - e_{33}^f k_{2j}^h) I_1(\xi_j a) A_j(\xi) - \frac{a\xi^2}{2} \left[ (c_{13}^f k_1^{pz} + e_{31}^f k_2^{pz}) \bar{\psi}^{pz}(\xi) + (c_{13}^f k_1^{pq} + e_{31}^f k_2^{pq}) \bar{\psi}^{pq}(\xi) \right] \right\} e^{-i\xi z} d\xi \quad (4.7)$$

The interfacial shear stress and the electric field along the  $z$ -axis are given by

$$\sigma_{rz}(a, z) = \frac{1}{\sqrt{2\pi}} \int_{-\infty}^{\infty} -i\xi \sum_{j=1}^3 \xi_j \left\{ c_{44}^f (1 + k_{1j}^h) - e_{15}^f k_{2j}^h \right\} I_1(\xi_j a) A_j(\xi) e^{-i\xi z} d\xi \quad (4.8a)$$

$$E_z(0, z) = \frac{1}{\sqrt{2\pi}} \int_{-\infty}^{\infty} \xi^2 \left\{ \sum_{j=1}^3 k_{2j}^h A_j(\xi) + k_2^{pz} \bar{\psi}^{pz}(\xi) + k_2^{pq} \bar{\psi}^{pq}(\xi) \right\} e^{-i\xi z} d\xi \quad (4.8b)$$

## 4.2 Numerical Results and Discussion

The computation of the electroelastic field corresponding to the problem shown in Figure 4.1 requires the numerical evaluation of the infinite integral given by equation (3.9b). This integral can be converted to a semi-infinite integral by using the symmetric and anti-symmetric properties of the integrands. In the present study, a globally adaptive numerical quadrature scheme is employed to evaluate the integral (Piessens et al., 1983). The scheme subdivides the interval of integration and uses a 21-point Gauss–Kronrod rule to estimate the integral over each subinterval. The error for each subinterval is estimated by comparing between the result obtained from 21-point Gauss–Kronrod rule and that from 10-point Gauss–Kronrod rule. The subinterval with the largest estimated error is then bisected, and this procedure is applied to both halves. This bisection procedure is continued until the error criterion is reached.

### 4.2.1 Comparison with Existing Solutions

The accuracy of the present scheme is first verified by comparing with the existing solutions for an ideal elastic composite system. The present solution scheme can be used to analyze the axial load transfer in an elastic fiber-reinforced composite by setting the piezoelectric coefficients of the fiber to negligibly small values ( $e_{ij} \approx 0$ ). Figure 4.2 presents a comparison of the numerical solutions for the fibre axial force of a perfectly bonded fiber with those presented by Muki and Sternberg (1969). The Poisson's ratios of the fiber and matrix are equal to 0.25, and  $E^f$  and  $E^m$  denote Young's moduli of the fiber and matrix respectively. The solutions presented in Figure 4.2 show an excellent agreement for various values of  $E^f / E^m$  confirming the accuracy of the present solution.

Further comparisons are presented by considering the case of elastic composites with imperfect fiber–matrix interfaces (Lenci & Menditto, 2000). The elastic modulus of the fiber,  $E^f = 68.954$  GPa, Poisson's ratio of the matrix

$\nu=0.34$  and shear modulus of the matrix  $\mu=2.59$  GPa. Lenci and Menditto (2000) simplified the analysis by modeling the fiber as a one-dimensional bar whereas the present solution allows the fiber to be considered as a three-dimensional continuum. A comparison of the fiber axial force, and interfacial shear and radial stresses are presented in Figure 4.3 for various nondimensional interface stiffness values,  $E^f/(k_s a)$ , in which  $k_s$  and  $a$  denote the interface stiffness (spring-factor) and radius of the fiber respectively. It can be seen from Figures 4.3(a) and (b) that the results given by Lenci and Menditto (2000) and the present scheme agree closely for the fiber axial force and interfacial shear stress. In the case of interfacial radial stress. Figure 4.3(c) shows two solutions obtained from the present scheme: one corresponding to full radial displacement compatibility between the fiber and matrix and the other with the constraint that interfacial radial displacement is zero. In the vicinity of the loading plane, the two solutions from the present scheme and the results of Lenci & Menditto (2000) agree closely but the differences are noted between the full radial displacement compatibility solution and the solution from Lenci & Menditto (2000) as the distance in  $z$ -direction increases. This is due to the fact that the radial deformation is not accounted by the 1-D fiber model of Lenci and Menditto (2000). On the other hand, the present solution for interfacial radial stress with the constraint  $u_r^f(a, z) = 0$  agrees very closely with the corresponding solution of Lenci and Menditto (2000) for all values of  $z/a$ .

#### 4.2.2 Force and Charge Diffusion in Piezocomposites

In this section, selected numerical solutions are presented to demonstrate the basic features of the electromechanical load diffusion process in piezoelectric fiber-reinforced composites. Two elastic polymer matrix materials, identified as matrix A and matrix B, with three different piezoelectric fibers, namely, PZT-6B, PZT-4 and BaTiO<sub>3</sub> are considered in the numerical study. The properties of these materials are given in Table 4.1.

The case of piezocomposites with perfect bonding along the fiber–matrix interface is first examined. The corresponding solutions are presented in Figures 4.4–4.9 for fibers with open– and short–circuited conditions along the interface. Note that solutions are presented only for  $z \geq 0$  as all quantities are either symmetric or anti–symmetric with respect to the loading plane  $z = 0$ .

Consider the diffusion of an axial load of magnitude  $P_0$  applied uniformly over the cross section at  $z=0$  of the fiber (Figure 4.1). The variation of nondimensional resultant axial force along the fiber length is shown in Figure 4.4(a) for the open–circuited case. Naturally, the nondimensional axial load has a unit magnitude at  $z=0$  and decreases gradually with  $z$ . The decay of axial load in the fiber depends on the type of fiber and matrix material. As the matrix A is stiffer than matrix B (Table 4.1), the axial load is more rapidly transferred to matrix A when compared to matrix B. For example, at a distance six times the fiber–radius from the loading plane, the fiber axial load is approximately 10% and 30% of the applied load for matrix A and matrix B respectively. The dependence of fiber axial load on fiber material properties is quite negligible when compared to its dependence on the matrix material properties.

In the case of piezocomposites, particular interest for sensor applications is the electric field generated in the fiber due to the applied mechanical loading. Figure 4.4(b) shows the nondimensional vertical electric field,  $E_z^* = E_z e_{15}^f a^2 / P_0$ , along the axis of the piezoelectric fiber. The peak value of vertical electric field occurs near the loading plane ( $z/a < 1$ ) and thereafter  $E_z^*$  gradually decreases with  $z$ . The decay of  $E_z^*$  along the fiber length is significantly affected by the properties of the fiber and matrix. The PZT–4 fiber has the highest  $E_z^*$  followed by the BaTiO<sub>3</sub> and PZT–6B fibers implying that PZT–4 is more suitable for applications involving sensing. A softer matrix material results in a higher vertical electric field in the fiber as lesser load is transferred to the matrix. In addition, the decay of electric field is relatively slow in the case of a softer matrix allowing better sensing properties.



The variations of nondimensional shear stress,  $\sigma_{rz}^* = \sigma_{rz} a^2 / P_0$ , and radial stress,  $\sigma_{rr}^* = \sigma_{rr} a^2 / P_0$ , along the fiber–matrix interface ( $r/a = 1$ ) are presented in Figures 4.5(a) and 4.5(b) respectively. Similar to the case of the fiber axial force, interfacial stresses are mostly influenced by the matrix material when compared to the properties of the fiber. Shear stress along the interface has its maximum value at the loading plane and decreases rapidly in the vertical (fiber) direction. Stiffer matrix materials result in higher interfacial stresses as the load transfer to the matrix is more rapid in this case. Consequently, such composites are more prone to interfacial failure provided that the shear strength at the interface is the same. Radial stress along the fiber–matrix interface is zero at  $z = 0$  and increases rapidly with  $z$  reaching a peak value near  $z/a = 1$  and thereafter decreases rapidly with  $z$ . The peak value of the interface radial stress is less than 10% of the peak interface shear stress. Therefore, interfacial strength is mostly governed by the cohesion at the interface instead of Coulomb friction in the present model.

Next, consider the diffusion of a patch electric charge from a fiber perfectly bonded to a matrix. Nondimensional vertical stress,  $\sigma_{zz}^{**} = \sigma_{zz} e_{15}^f a^2 / c_{44}^f Q_0$ , and vertical electric field,  $E_z^{**} = E_z (e_{15}^f)^2 a^2 / c_{44}^f Q_0$ , along the  $z$ -axis are presented in Figures 4.6(a) and 4.6(b) respectively. A substantial dependence of vertical stress on the fiber type is noted. Vertical stress is zero at the loading plane and initially increases rapidly and then decreases slowly along the fiber axis. It is tensile along the upper fiber length, and PZT-4 has the highest nondimensional value. Figure 4.6(b) shows the variation of  $E_z^{**}$  along the fiber axis. In this case, BaTiO<sub>3</sub> and PZT-6B fibers have nearly equal but substantially smaller values of  $E_z^{**}$  when compared to a PZT-4 fiber. The decay of the vertical electric field along the fiber length is not rapid. Nondimensional shear stress,  $\sigma_{rz}^{**} = \sigma_{rz} e_{15}^f a^2 / c_{44}^f Q_0$ , and radial stress,  $\sigma_{rr}^{**} = \sigma_{rr} e_{15}^f a^2 / c_{44}^f Q_0$ , at the fiber–matrix interface due to an electric charge are shown in Figures 4.7(a) and 4.8(b) respectively. The variation of shear and radial

stresses along the interface is somewhat similar to the results shown in Figure 4.5. However, the dependence of the interface stresses on the fiber and matrix material type is more pronounced in the case of electric charge loading when compared to the axial loading.

Figure 4.8 shows the resultant axial force and vertical electric field of a short-circuited fiber bonded to an elastic matrix due to an axial force  $P_0$ . The axial force profiles are similar to those shown in Figure 4.4(a) but the load transfer is slightly more rapid than the open-circuited case and the influence of the fiber properties on the force profiles are higher. Vertical electric field decays very rapidly along the fiber length in contrast to Figure 4.4(b) and show less dependence on the matrix material. The interfacial stresses for the short-circuited case show similar behavior to Figure 4.5 but the magnitudes are higher by 20–50%. Figure 4.9 shows the variation of vertical stress and vertical electric field when a short-circuited fiber is subjected to an electric charge  $Q_0$ . The profiles are very different from those shown in Figure 4.6 and show very rapid decay of axial stress and vertical electric field along the fiber length. The magnitudes show considerable dependence on the fiber properties but negligible influence of matrix material. As in the case of Figure 4.6 the maximum values of nondimensional axial stress and vertical electric field correspond to PZT-4. Comparisons with Figure 4.6 also shows that axial stress and vertical electric field are much smaller in the short-circuited case.

Figures 4.10(a) and 4.10(b) show the nondimensional shear stress along the  $r$ -axis at the  $z=0$  plane, and the nondimensional radial stress at  $z/a=1$  respectively, due to the axial load applied to the open-circuited piezoelectric fiber-reinforced composites. The radial variations of shear stress at  $z=0$  and radial stresses at  $z/a=1$  for piezocomposites under an applied electric charge are also presented in Figures 4.11(a) and 4.11(b) respectively. It is evident from Figures 4.10 and 4.11 that the stresses profiles decrease rapidly along the transverse direction. At  $r/a=4$ , which corresponds to the fiber-to-fiber distance

for the optimized piezoelectric volume fraction of 20%, the shear and radial stresses reduce to relatively small values when compared to the corresponding values at  $r/a=1$  for both electric charge and axial load cases. The radial profiles of stress fields for the closed-circuited piezoelectric fiber-reinforced composites are also investigated and show the similar behavior as the opened-circuited case. The solutions in transverse direction shown in Figures 4.10 and 4.11 confirm that the assumption of negligible fiber-to-fiber effect is reasonable for the analysis of piezoelectric fiber-reinforced composites and the 1-3 piezocomposite (Figure 1.1) can be modeled by an infinite elastic matrix with a single piezoelectric fiber as shown in Figure 3.1.

The effect of imperfect fiber-matrix bonding on the load diffusion characteristics is presented in Figures 4.12–4.15. Two cases of piezocomposites are considered in the numerical study, i.e., composites of PZT-6B fiber with matrix A and PZT-4 fiber with matrix B. The interface behavior is characterized by the spring-factor model described in equation (4.3b). Five values of nondimensional spring-factor,  $k_s^* = (k_s a) / c_{44}^f = 10, 1, 0.1, 0.01$  and  $0.001$  are considered in the numerical study. Figures 4.12 and 4.13 show the electroelastic field of composites of PZT-6B fiber with matrix A and PZT-4 fiber with matrix B respectively under an applied axial load. Numerical results presented in Figures 4.12 and 4.13 demonstrate a substantial dependence of the electroelastic field of both composites on the interface stiffness. Figures 4.12(a) and 4.13(a) shows that fiber axial force significantly depends on the stiffness of the interface and as  $k_s^*$  decreases (weaker interface) the load transferred to the matrix is obviously reduced. The magnitudes of interfacial shear stress and radial stress obviously decrease as the interface bonding becomes weaker and the decay along the interface becomes less rapid. On the other hand, vertical electric field of the fiber increases in the case of a weaker interface due to less load transfer to the matrix. The magnitude of fiber vertical electric field can be considered as a measure of the interface condition (weaker interface yields a higher fiber electric field).

Therefore, it is possible to obtain a qualitative non-destructive assessment of the interface bond condition by comparing vertical electric field of fibers. A comparison of Figures 4.12 and 4.13 indicates that an imperfect interface has a relatively lesser effect on the load diffusion in a PZT-4/Matrix B composite and the interfacial stresses are also smaller.

The effect of an imperfect interface on electric charge transfer is shown in Figure 4.14 for a composite of PZT-6B fibers with matrix A and in Figure 4.15 for a composite of PZT-4 fibers with matrix B. The influence of interface bonding condition is relatively small when compared to the effects observed in Figures 4.12 and 4.13 for an axial load. Vertical electric field is negative, and its absolute value is increased as the interface becomes weaker. The fiber tensile axial stress is also increased as the interface becomes weaker. However, near the loading plane vertical stress and electric field show negligible influence of the interface stiffness. Nondimensional shear and radial stresses indicate that interfacial stresses decrease as the interface becomes weaker similar to the behavior observed for the axial load diffusion but the stresses have signs opposite to those corresponding to the axial load transfer case. A comparison of Figures 4.14 and 4.15 shows that the influence of interface stiffness is less in the case of PZT-4/Matrix B composites under electric charge loading similar to the case of axial loading.

Table 4.1 Material properties used in the numerical study

	PZT-6B	PZT-4	BaTiO3	Matrix A	Matrix B
$c_{11}$ ( $\times 10^{10}$ N/m <sup>2</sup> )	16.8	13.9	15.0	1.49	0.2827
$c_{33}$ ( $\times 10^{10}$ N/m <sup>2</sup> )	16.3	11.5	14.6	4.72	0.2827
$c_{12}$ ( $\times 10^{10}$ N/m <sup>2</sup> )	6.0	7.78	6.6	0.66	0.1211
$c_{13}$ ( $\times 10^{10}$ N/m <sup>2</sup> )	6.0	7.43	6.6	0.52	0.1200
$c_{44}$ ( $\times 10^{10}$ N/m <sup>2</sup> )	2.71	2.56	4.4	0.47	0.0808
$e_{31}$ (C/m <sup>2</sup> )	-0.9	-5.2	-4.35	0.0	0.0
$e_{33}$ (C/m <sup>2</sup> )	7.1	15.1	17.5	0.0	0.0
$e_{15}$ (C/m <sup>2</sup> )	4.6	12.7	11.4	0.0	0.0
$\epsilon_{11}$ ( $\times 10^{-9}$ F/m)	3.6	6.45	9.87	0.0	0.0
$\epsilon_{33}$ ( $\times 10^{-9}$ F/m)	3.4	5.62	11.15	0.0	0.0

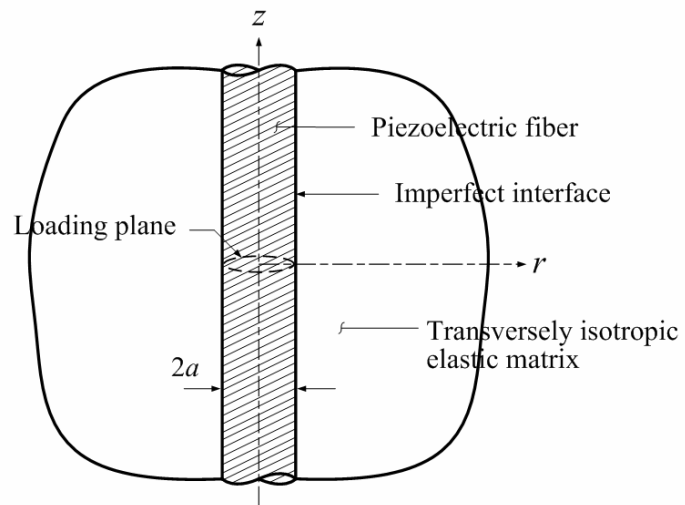


Figure 4.1 A piezoelectric fiber-reinforced composite with imperfect interface.

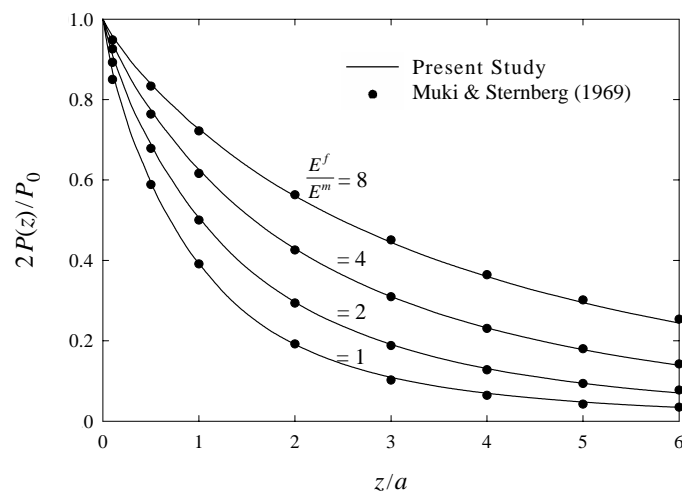


Figure 4.2 Comparison of the fiber axial force for elastic composites with perfect interface.

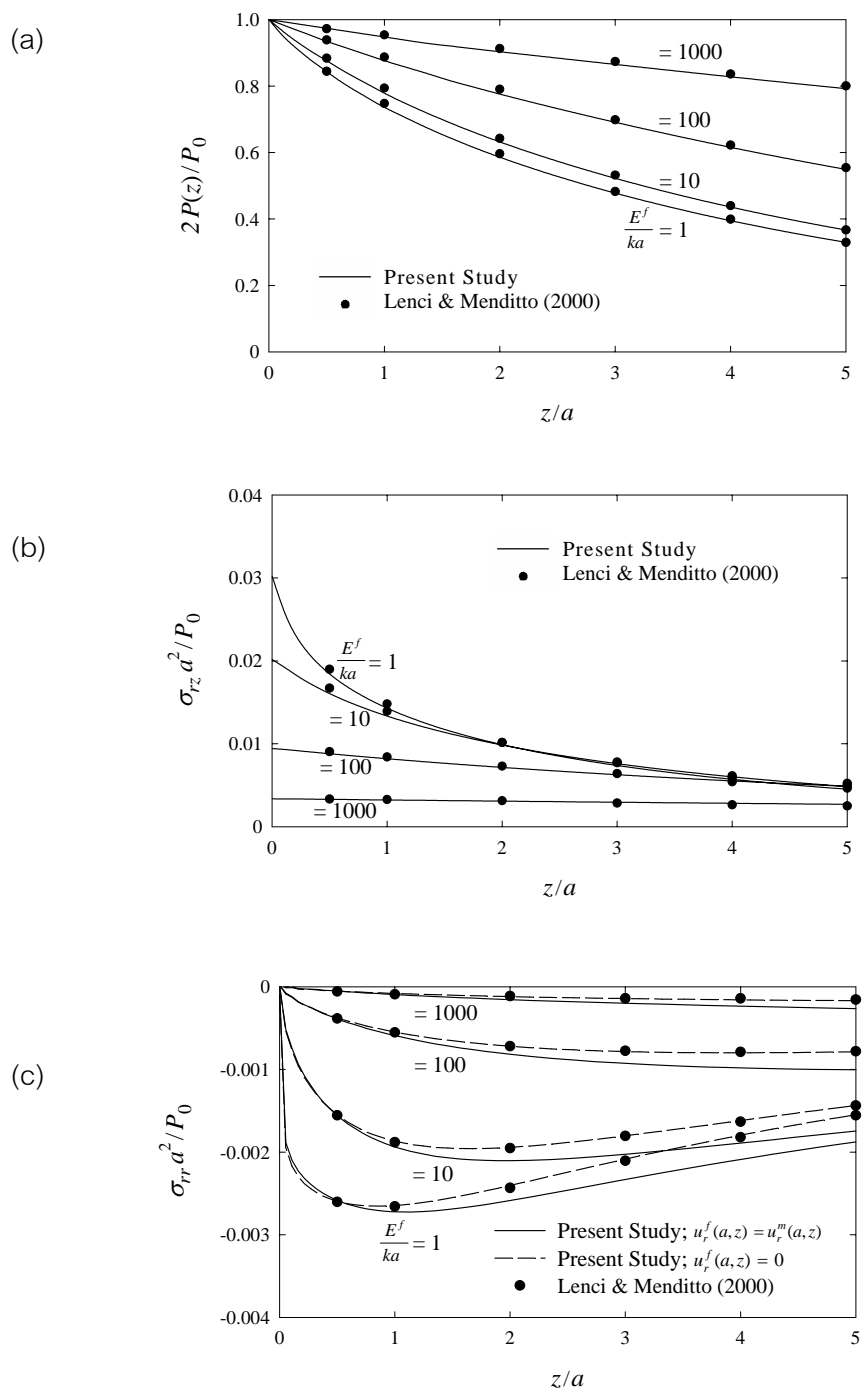
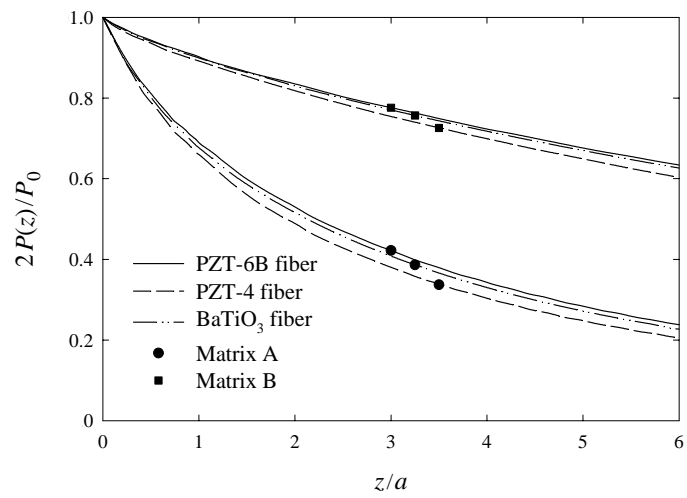
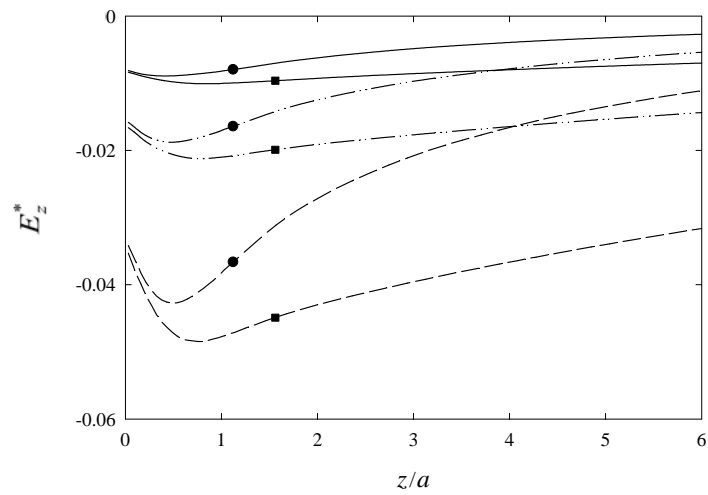


Figure 4.3 Comparison of (a) fiber axial force; (b) interfacial shear stress and (c) interfacial radial stress for elastic composite with imperfect interface.



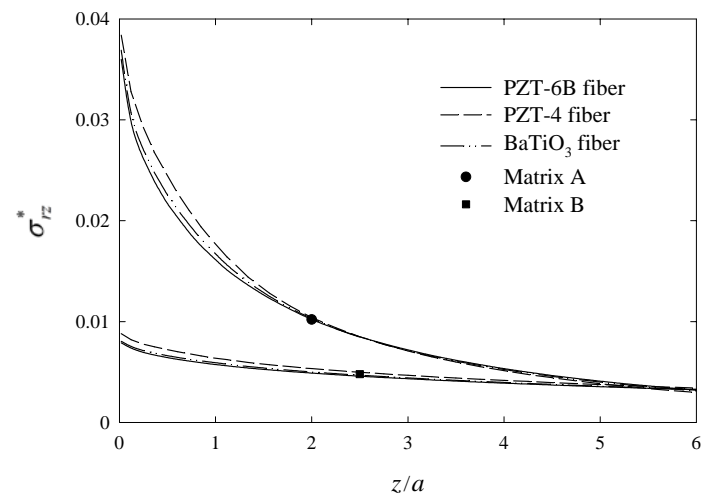
(a)



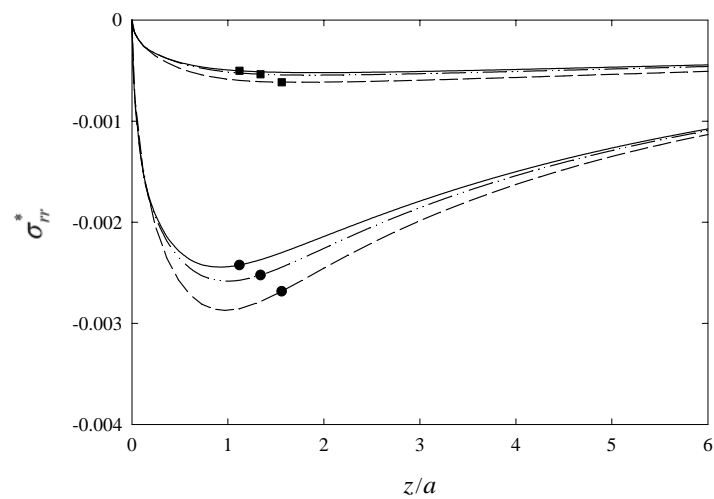
(b)

Figure 4.4 (a) Resultant axial force and (b) vertical electric field along the  $z$ -axis of piezoelectric fiber (open-circuited) under applied axial load.



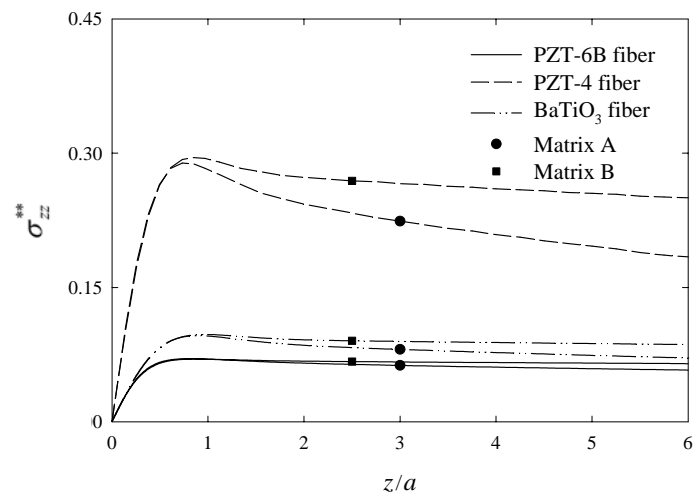


(a)

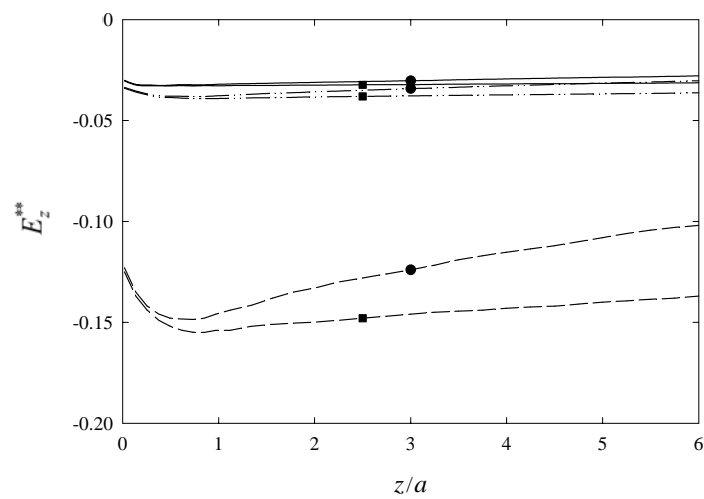


(b)

Figure 4.5 (a) Shear and (b) radial stresses along the fiber–matrix interface of piezoelectric composite (open–circuited) under applied axial load.

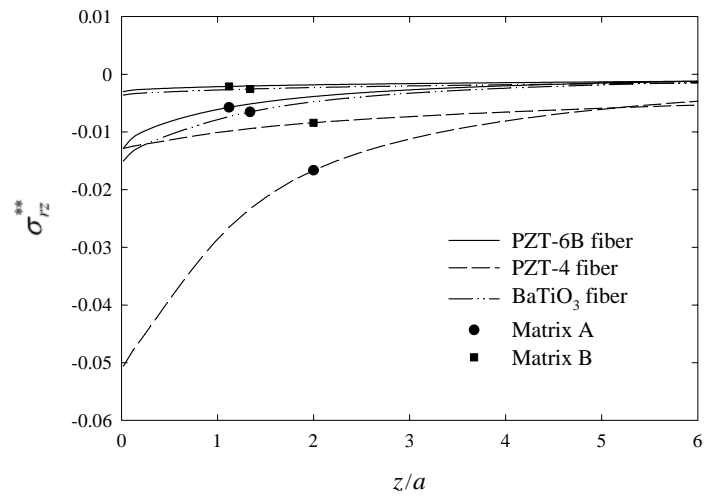


(a)

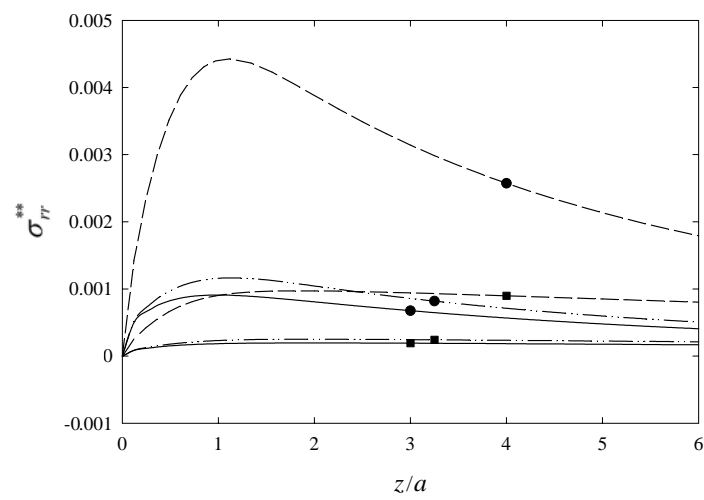


(b)

Figure 4.6 (a) Vertical stress and (b) vertical electric field along the  $z$ -axis of piezoelectric fiber (open-circuited) under applied electric charge.

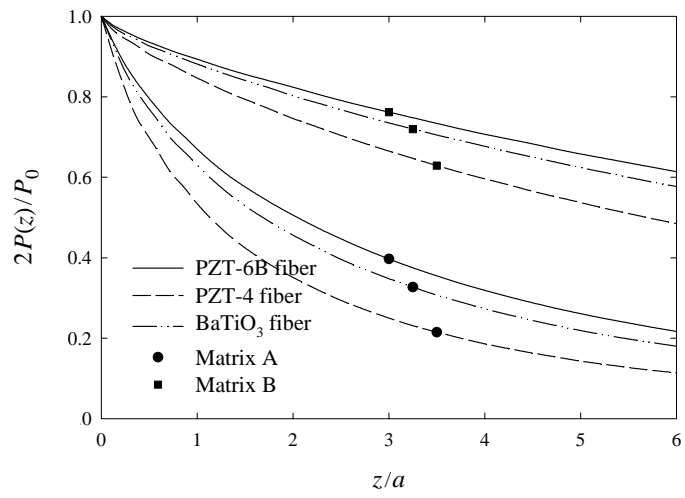


(a)

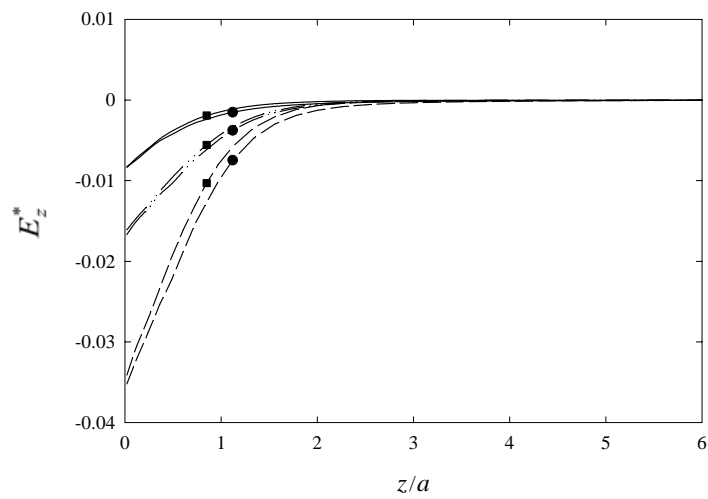


(b)

Figure 4.7 (a) Shear and (b) radial stresses along the fiber–matrix interface of piezoelectric composite (open–circuited) under applied electric charge.

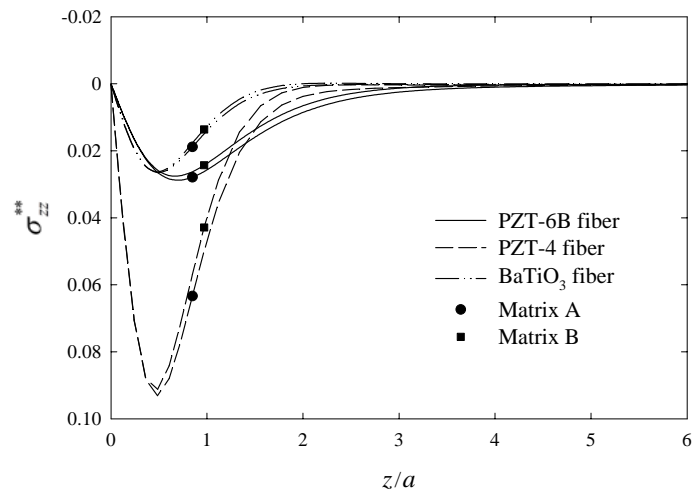


(a)

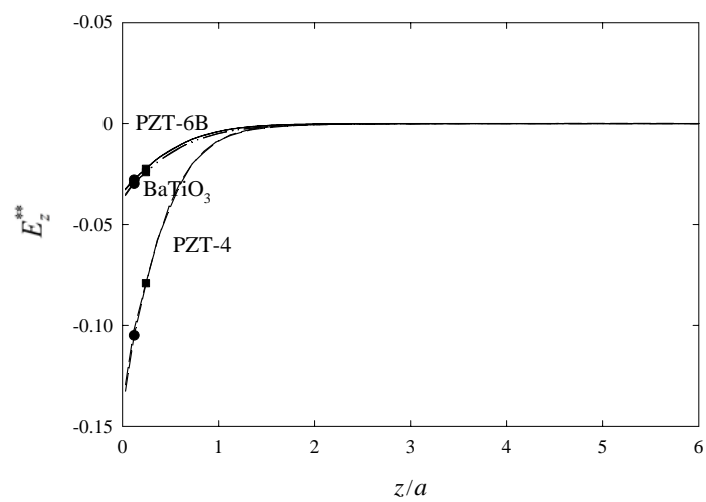


(b)

Figure 4.8 (a) Resultant axial force and (b) vertical electric field along the  $z$ -axis of piezoelectric fiber (short-circuited) under applied axial load.

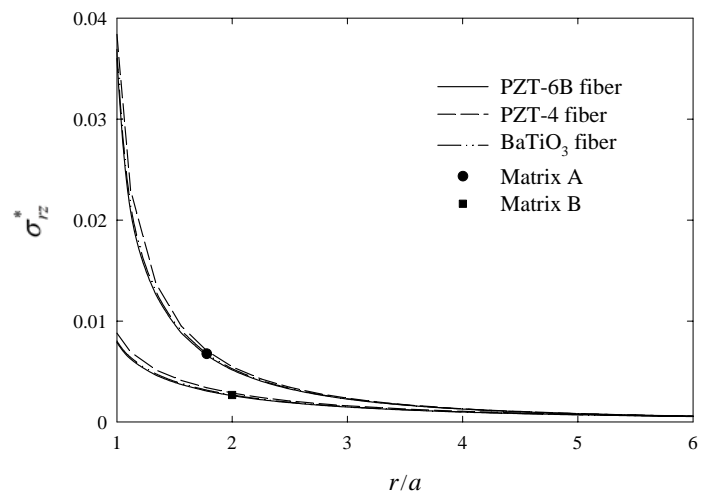


(a)

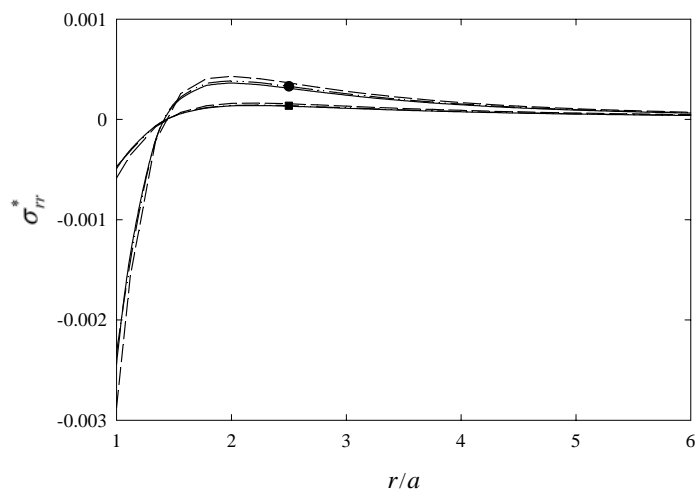


(b)

Figure 4.9 (a) Vertical stress and (b) vertical electric field along the  $z$ -axis of piezoelectric fiber (short-circuited) under applied electric charge.

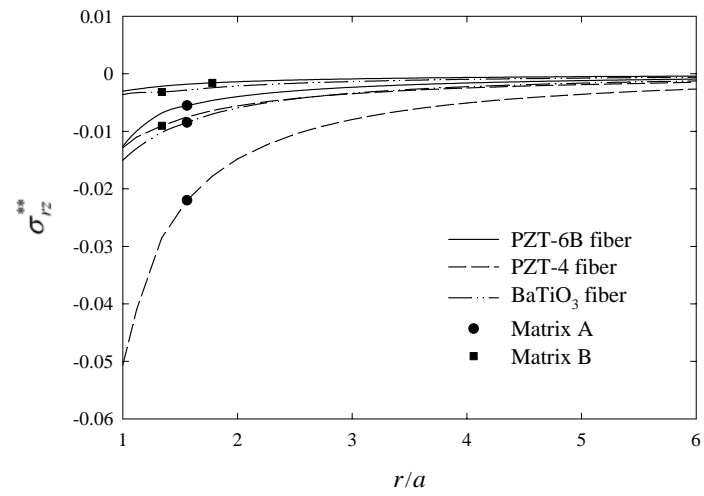


(a)

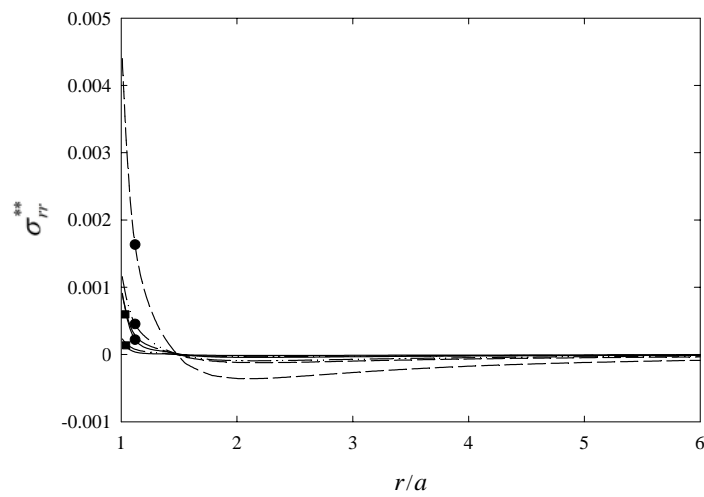


(b)

Figure 4.10 (a) Shear stress profiles along the  $r$ -axis at  $z=0$  and (b) radial stress profiles along the  $r$ -axis at  $z/a=1$  (open-circuited) under applied axial load.



(a)



(b)

Figure 4.11 (a) Shear stress profiles along the  $r$ -axis at  $z=0$  and (b) radial stress profiles along the  $r$ -axis at  $z/a=1$  (open-circuited) under applied electric charge.

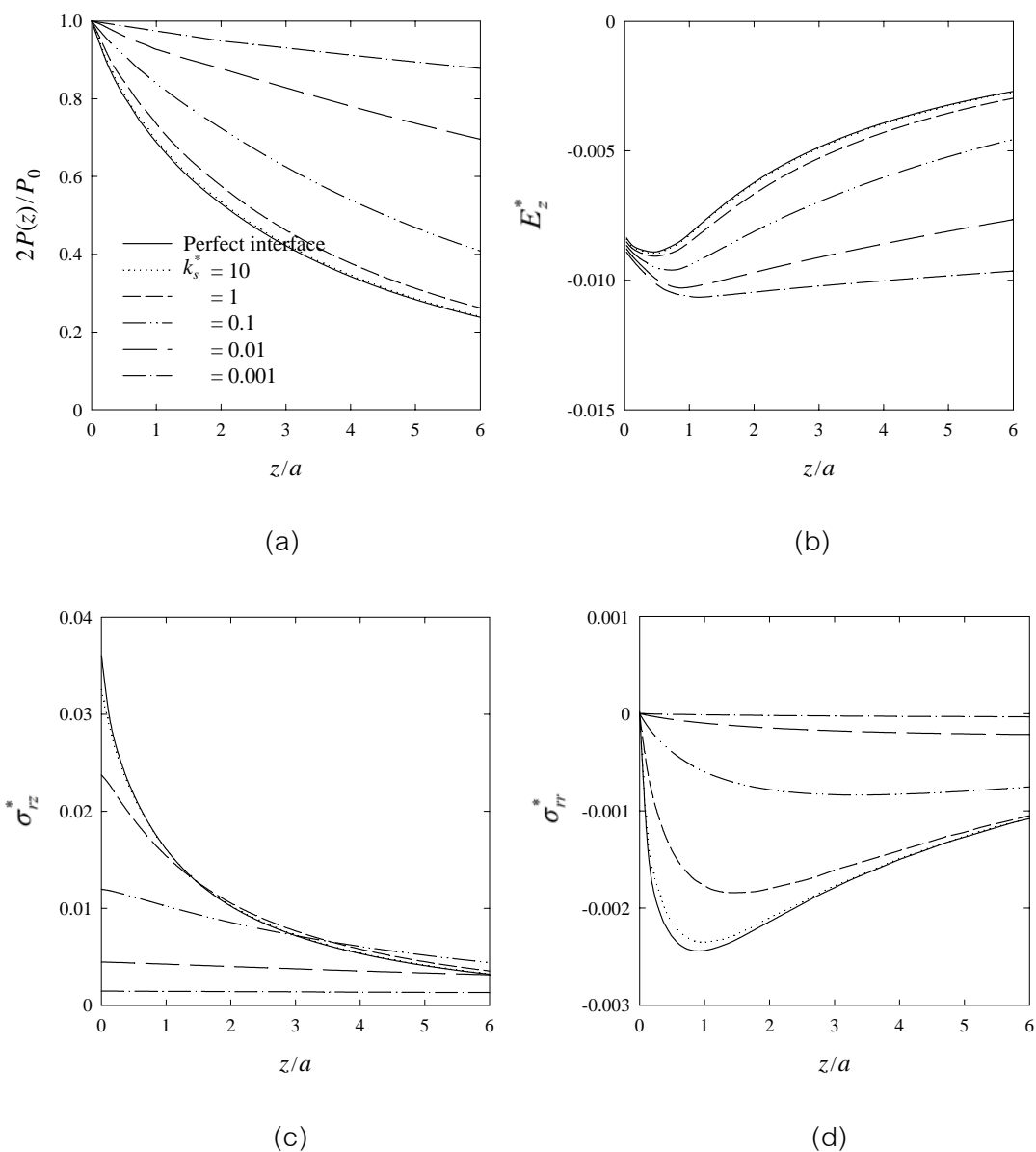


Figure 4.12 Composite of PZT-6B fiber with Matrix A (a) resultant axial force and (b) vertical electric field along the  $z$ -axis of piezoelectric fiber; (c) shear and (d) radial stresses along the fiber-matrix interface (open-circuited) under applied axial load for different interface stiffness values.



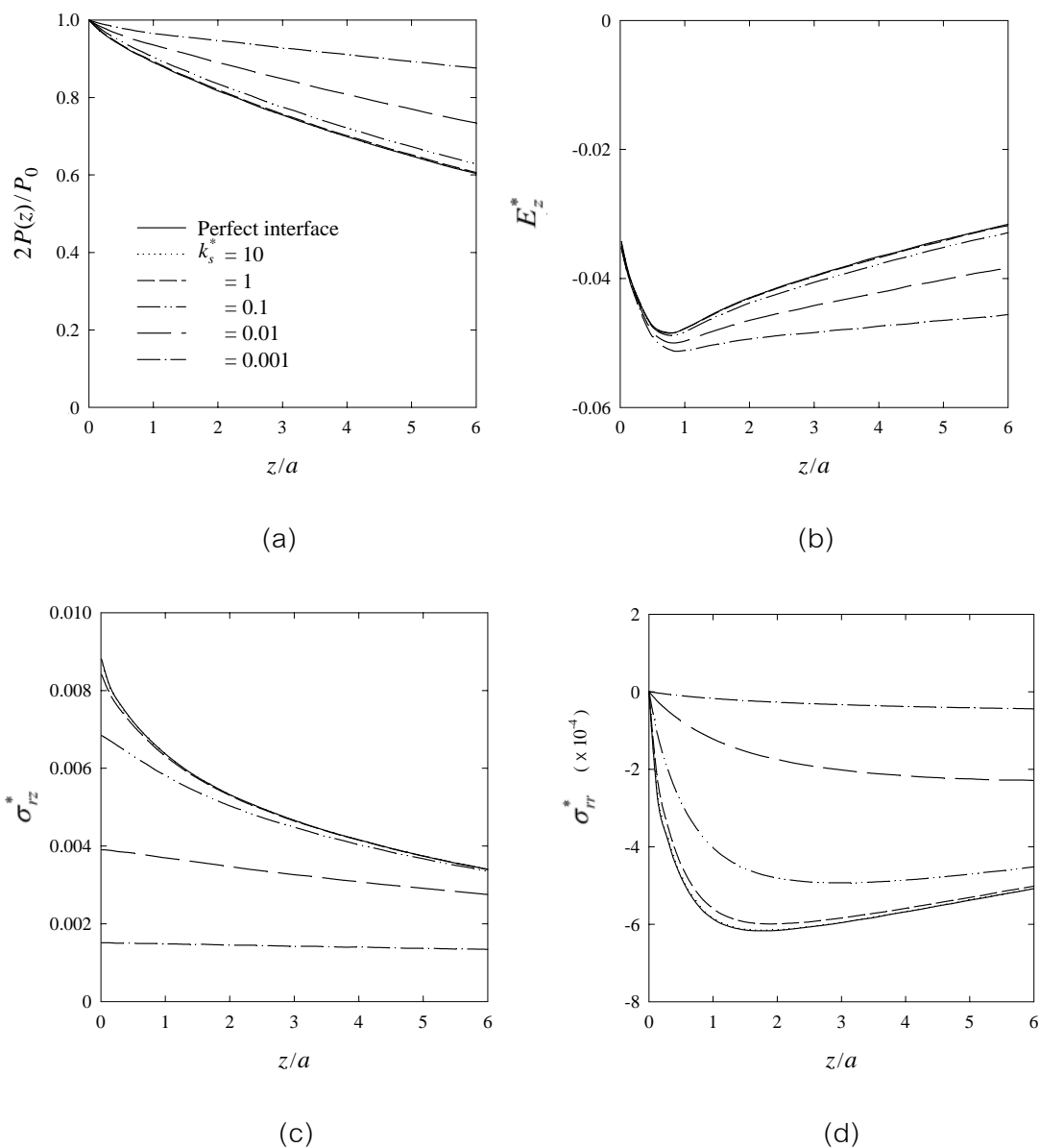


Figure 4.13 Composite of PZT-4 fiber with Matrix B (a) resultant axial force and (b) vertical electric field along the  $z$ -axis of piezoelectric fiber; (c) shear and (d) radial stresses along the fiber-matrix interface (open-circuited) under applied axial load for different interface stiffness values.

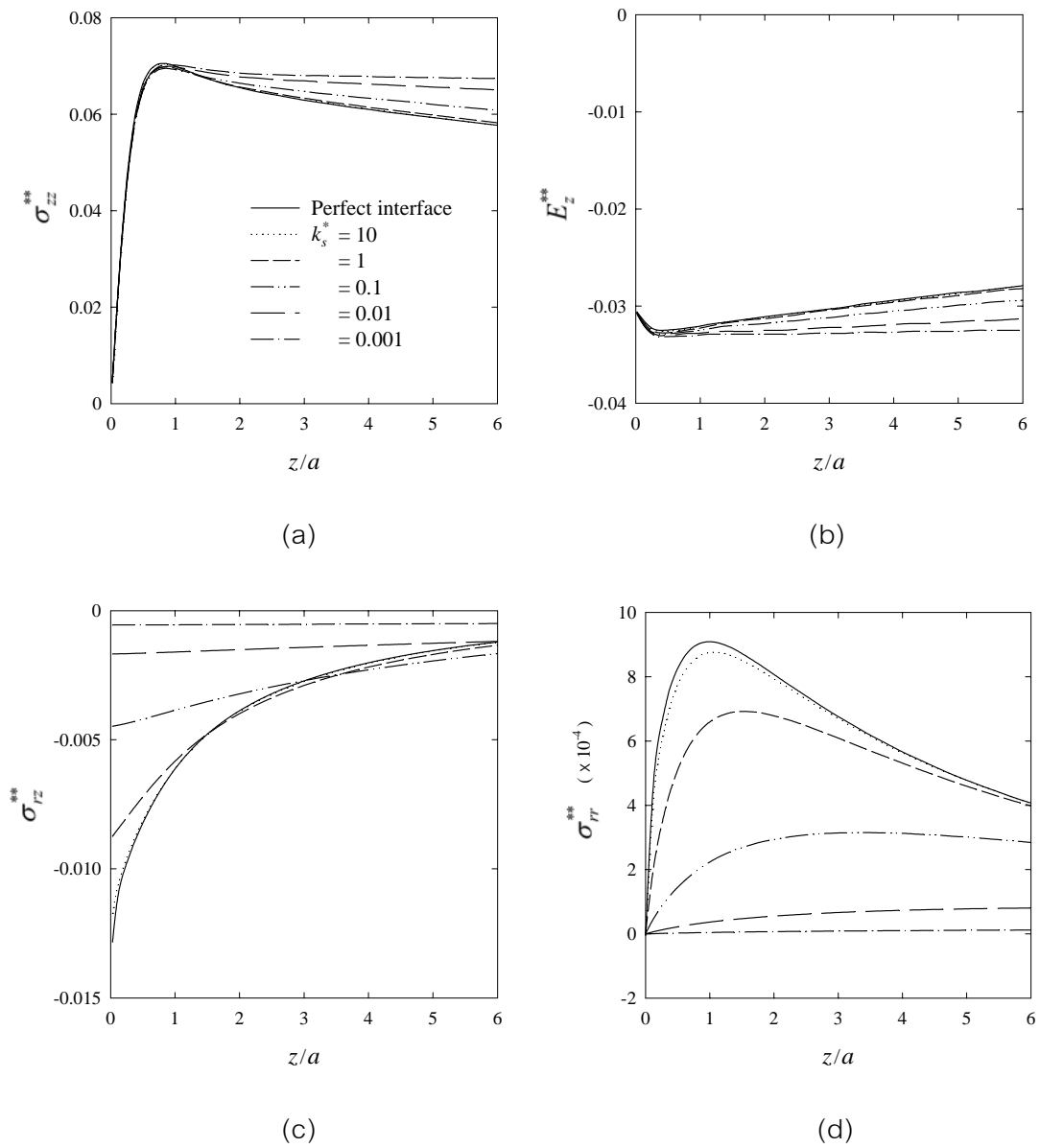


Figure 4.14 Composite of PZT-6B fiber with Matrix A (a) vertical stress and (b) vertical electric field along the  $z$ -axis of piezoelectric fiber; (c) shear and (d) radial stresses along the fiber-matrix interface of piezoelectric composite (open-circuited) under applied electric charge for different interface stiffness values.

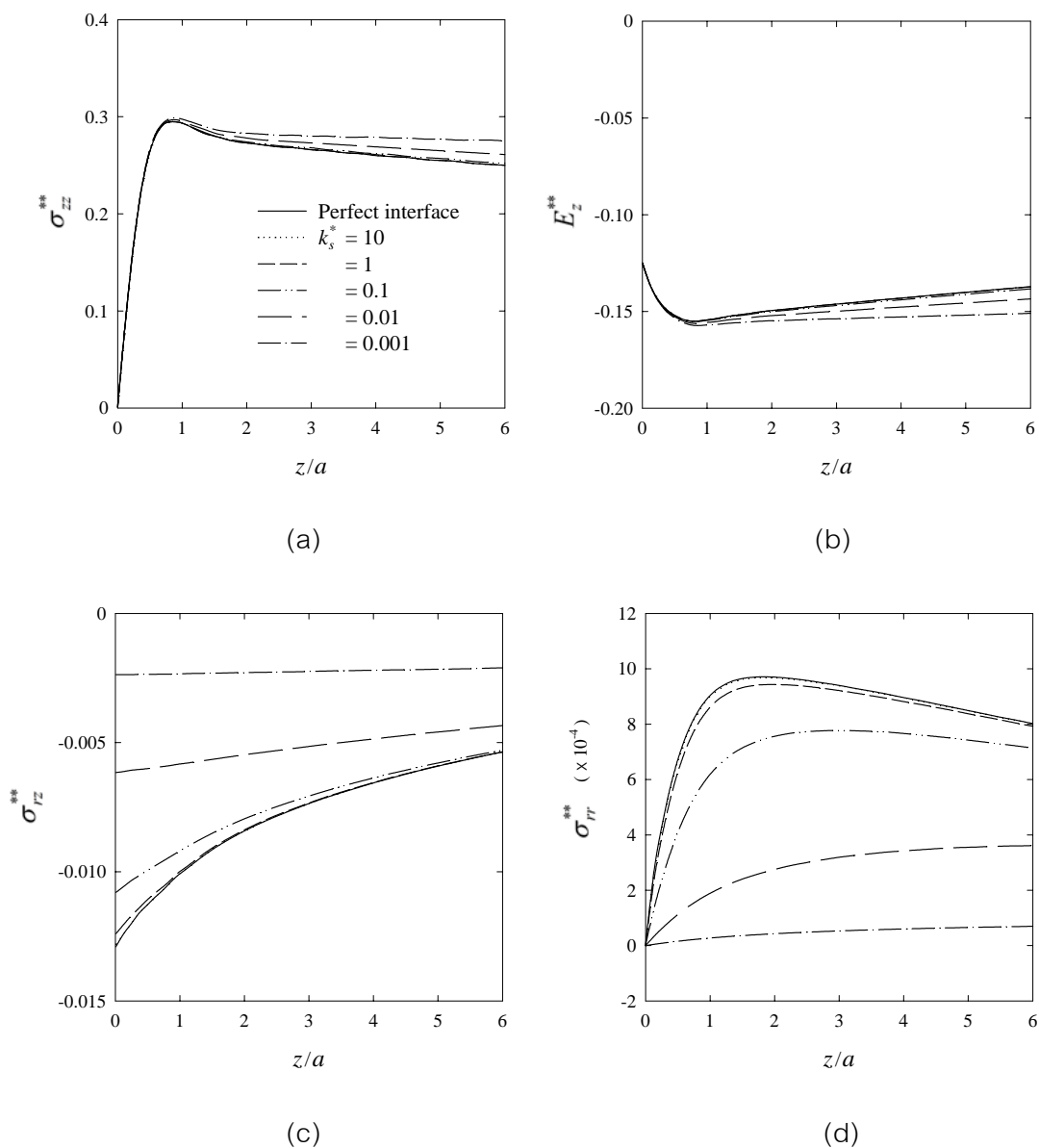


Figure 4.15 Composite of PZT-4 fiber with Matrix B (a) vertical stress and (b) vertical electric field along the  $z$ -axis of piezoelectric fiber; (c) shear and (d) radial stresses along the fiber-matrix interface of piezoelectric composite (open-circuited) under applied electric charge for different interface stiffness values.

## CHAPTER V

### CYLINDRICAL INTERFACE CRACK IN PIEZOCOMPOSITES

In this chapter, three-dimensional axisymmetric interface crack in a piezoelectric fiber-reinforced composite is examined by adopting the displacement discontinuity method (DDM) based on the fundamental solutions of interface dislocations. The general solutions of piezoelectric fiber and elastic matrix presented in chapter 3 are used to derive the required fundamental solutions of interface dislocations. A special crack tip element is introduced in the DDM formulation for improving the accuracy of the field quantities in the vicinity of the crack tip. The explicit solutions interface dislocations are given. The mathematical implementation and the intensity factors for interface crack in piezocomposite are discussed. The validity of the present scheme is confirmed by comparison with existing solutions for elastic case reported in the literature. Selected numerical results for crack opening displacements and field intensity factors are presented and discussed.

#### 5.1 Problem Formulation

Consider a piezocomposite that consists of a cylindrical piezoelectric fiber of radius " $a$ " perfectly bonded to an elastic matrix but contains a cylindrical interface crack of length " $2c$ " as shown in Figure 5.1. The piezoelectric fiber and the elastic matrix are assumed to be transversely isotropic, and the boundary condition along the fiber interface is electrically impermeable. A polar co-ordinate system is used in which  $z$ -axis coincides with the principal axis of transversely isotropy. The displacement discontinuity method (DDM), originally developed for plane elasticity, is extended for the analysis of this fracture problem. The DDM analysis of the interface crack requires fundamental solutions of the interface dislocation in a piezocomposite as shown in Figure 5.3. The analytical general solutions corresponding to piezoelectric fiber and an elastic

matrix presented in Chapter 3 are used to determine the required fundamental solutions for the present scheme. Details on the DDM formulation and derivation of the fundamental solutions are explained in the subsequent sections.

### 5.1.1 Displacement Discontinuity Method (DDM)

The displacement discontinuity method (DDM), introduced by Crouch and Starfield (1983), is extended for the analysis of interface crack in a piezocomposite as shown in Figure 5.1. Based on the DDM formulation, the crack surface is subdivided into  $N$  segments as shown in Figure 5.2. Each segment contains a constant displacement discontinuity  $d_i$  ( $i = r, z$ ), which is defined by

$$d_i = u_i^f(a, z) - u_i^m(a, z), \quad i = r, z \quad (5.1)$$

The influence of a single displacement discontinuity from each element on the field quantities at an arbitrary point in the material can be determined. Specifically, the radial and tangential stresses at the midpoint of the  $i$ th element can be expressed in terms of the displacement discontinuity components at the  $j$ th element as

$$\left. \begin{aligned} \sigma_{rr}^i &= A_{rr}^{ij} d_r^j + A_{rz}^{ij} d_z^j \\ \sigma_{rz}^i &= A_{zr}^{ij} d_r^j + A_{zz}^{ij} d_z^j \end{aligned} \right\} i, j = 1, 2, \dots, N \quad (5.2)$$

where  $A_{rr}^{ij}$ ,  $A_{rz}^{ij}$ ,  $A_{zr}^{ij}$  and  $A_{zz}^{ij}$  are the influence coefficients for the stresses along the fiber–matrix interface. For example, the coefficient  $A_{rz}^{ij}$  represents the interface radial stress ( $\sigma_{rr}$ ) at the midpoint of the  $i$ th element due to a unit displacement discontinuity ( $d_z=1$ ) over the  $j$ th element. These influence coefficients can be obtained from the fundamental solutions of interface dislocations in a piezocomposite in which the explicit solutions are given in section 5.1.2.

The specified values of the radial and tangential stresses for each element,  $\sigma_{rr}^i$  and  $\sigma_z^i$ , lead to a system of  $2N$  linear equations for  $2N$  unknowns,

which are the elemental displacement discontinuity components  $d_r^i$  and  $d_z^i$ . After solving the above equations for  $d_r^i$  and  $d_z^i$  ( $i = 1, 2, \dots, N$ ), the displacements, stresses and electric field at designated points in the composite material can be determined by considering the corresponding influence functions, given by equation (3.16) for the fiber and equation (3.17) for the matrix respectively, together with the principle of superposition.

### 5.1.2 Fundamental Solutions for Interface Dislocations

The required influence coefficients in equation (5.2) are determined from the fundamental solutions of elemental interface dislocation in a piezocomposite as shown in Figure 5.3. The general solutions of piezoelectric fiber and elastic matrix presented in chapter 3 are used to determine these fundamental solutions. Details on the derivation of the fundamental solutions for interface dislocation in piezocomposite are given in the following subsections.

#### 5.1.2.1 Radial Interface Dislocation

Consider a piezoelectric fiber–reinforced composite with constant radial displacement discontinuity,  $d_r$ , of a finite cylindrical region with radius “ $a$ ” and length “ $2h$ ” at the fiber–matrix interface (Figure 5.3). The fiber–matrix interface is assumed to be electrically impermeable and perfectly bonded. The boundary and continuity conditions along the fiber–matrix interface ( $r = a$ ) can be expressed as

*Displacement continuity*

$$u_r^f(a, z) - u_r^m(a, z) = d_r [H(z+h) - H(z-h)] \quad (5.3a)$$

$$u_z^f(a, z) - u_z^m(a, z) = 0 \quad (5.3b)$$

*Stress continuity*

$$\sigma_{rr}^f(a, z) - \sigma_{rr}^m(a, z) = 0 \quad (5.3c)$$

$$\sigma_{rz}^f(a, z) - \sigma_{rz}^m(a, z) = 0 \quad (5.3d)$$

*Electrical boundary condition*

$$D_r^f(a, z) = 0 \quad (5.3e)$$

where  $H(\ )$  denotes the Heaviside step function. Note that the superscript “ $f$ ” and “ $m$ ” are used to identify the quantities corresponding to the fiber ( $0 \leq r \leq a$ ) and matrix ( $a \leq r < \infty$ ) respectively.

The general solutions of piezoelectric fiber and elastic matrix are expressed by equation (3.16) with arbitrary functions  $A_1$ ,  $A_2$  and  $A_3$  and equation (3.17) with arbitrary  $C_1$  and  $C_2$  respectively. Application of Fourier integral transform to equation (5.3), the substitution of general solutions and after lengthy manipulations result in the following solutions for arbitrary functions  $A_1$ ,  $A_2$ ,  $A_3$ ,  $C_1$  and  $C_2$  as follows.

$$A_1 = d_r \{ I_{a1} h_{a1} \gamma_1 + [I_{a1} p_{a1} + h_{b1}(I_{b1} + I_{c1})] \gamma_2 + p_{b1}(I_{a1} + I_{b1}) \gamma_2 \} / W \quad (5.4a)$$

$$A_2 = -d_r \{ I_{a2} h_{a2} \gamma_1 + [I_{a2} p_{a2} + h_{b2}(I_{b2} + I_{c2})] \gamma_2 + p_{b2}(I_{a2} + I_{b2}) \gamma_2 \} / W \quad (5.4b)$$

$$A_3 = d_r \{ I_{a3} h_{a3} \gamma_1 + [I_{a3} p_{a3} + h_{b3}(I_{b3} + I_{c3})] \gamma_2 + p_{b3}(I_{a3} + I_{b3}) \gamma_2 \} / W \quad (5.4c)$$

$$C_1 = d_r \{ K_{02} n_2 (\gamma_4 + \gamma_5) + (s_2 K_{12} + |\xi| y_{12} K_{02}) \gamma_6 \} / W \quad (5.4d)$$

$$C_2 = -d_r \{ K_{01} n_1 (\gamma_4 + \gamma_5) + (s_1 K_{11} + |\xi| y_{11} K_{01}) \gamma_6 \} / W \quad (5.4e)$$

where

$$\begin{aligned} W = & \beta_1 \left[ \{ K_{02} K_{11} n_2 s_1 - K_{01} K_{12} n_1 s_2 + |\xi| K_{01} K_{02} (n_2 y_{11} - n_1 y_{12}) \} \right. \\ & + \beta_1 K_{02} K_{11} n_2 y_{11} - \beta_2 K_{01} K_{12} n_1 y_{22} + |\xi| \gamma_6 K_{11} K_{12} (s_2 w_1 - s_1 w_2) \\ & + |\xi|^2 \gamma_6 \{ K_{01} K_{12} w_2 y_{11} - K_{02} K_{11} w_1 y_{12} + K_{11} K_{12} (w_2 y_{21} - w_1 y_{22}) \} \\ & \left. + |\xi| \{ (\gamma_4 + \gamma_5) (K_{02} K_{11} n_2 w_1 - K_{01} K_{12} n_1 w_2 + \} \right] / (\sqrt{2/\pi} \sin(\xi h) / \xi) \end{aligned} \quad (5.5)$$

The functions appearing in equations (5.4)–(5.5) are related to the fiber and matrix’s material properties and given in Appendix B.

### 5.1.2.2 Axial Interface Dislocation

The boundary and continuity conditions along the fiber–matrix interface for this case can be expressed as

*Displacement continuity*

$$u_r^f(a, z) - u_r^m(a, z) = 0 \quad (5.6a)$$

$$u_z^f(a, z) - u_z^m(a, z) = d_z [H(z+h) - H(z-h)] \quad (5.6b)$$

*Stress continuity*

$$\sigma_{rr}^f(a, z) - \sigma_{rr}^m(a, z) = 0 \quad (5.6c)$$

$$\sigma_{rz}^f(a, z) - \sigma_{rz}^m(a, z) = 0 \quad (5.6d)$$

*Electrical boundary condition*

$$D_r^f(a, z) = 0 \quad (5.6e)$$

A procedure identical to the case of the radial displacement discontinuity results in the following solutions for arbitrary functions  $A_1$ ,  $A_2$ ,  $A_3$ ,  $C_1$  and  $C_2$ :

$$A_1 = d_z \left\{ \left[ \xi \left| I_{a1} (h_{a1} \gamma_7 + \gamma_8) + k_d (w_1 y_{22} - w_2 y_{21}) \right| \left[ \xi \left| I_{a1} p_{a1} + (I_{b1} + I_{c1}) h_{b1} \right| \right] \right\} / W \quad (5.7a)$$

$$A_2 = -d_z \left\{ \left[ \xi \left| I_{a2} (h_{a2} \gamma_7 + \gamma_8) + k_d (w_1 y_{22} - w_2 y_{21}) \right| \left[ \xi \left| I_{a2} p_{a2} + (I_{b2} + I_{c2}) h_{b2} \right| \right] \right\} / W \quad (5.7b)$$

$$A_3 = d_z \left\{ \left[ \xi \left| I_{a3} (h_{a3} \gamma_7 + \gamma_8) + k_d (w_1 y_{22} - w_2 y_{21}) \right| \left[ \xi \left| I_{a3} p_{a3} + (I_{b3} + I_{c3}) h_{b3} \right| \right] \right\} / W \quad (5.7c)$$

$$C_1 = d_z \left\{ \left[ \xi \left| K_{12} w_2 (\gamma_4 + \gamma_5) + (K_{12} s_2 + \left| \xi \left| K_{02} y_{12} \right| \right) \beta_1 + K_{12} y_{22} \beta_2 \right] \right\} / W \quad (5.7d)$$

$$C_2 = -d_z \left\{ \left[ \xi \left| K_{11} w_1 (\gamma_4 + \gamma_5) + (K_{11} s_1 + \left| \xi \left| K_{01} y_{11} \right| \right) \beta_1 + K_{11} y_{21} \beta_2 \right] \right\} / W \quad (5.7e)$$

### 5.1.3 Order of Singularity and Field Intensity Factors

The field intensity factor is an important concept in fracture mechanics. This invariant nature of the crack tip stresses reduces the analysis to the determination of the intensity factors for the specific problem of interest. Analytical solutions to the problem of crack in a homogeneous material show that



the stress fields in the neighborhood of a crack tip have square root singularities. The interface crack in composite bi-materials may contain singularity beside the classical square root. The order of singularity for the interface crack can be determined by using Stroh's formulation or Lekhnitskii's approach. It is noted that the order of singularity for the crack can be determined using any orthogonal coordinate system and therefore the axisymmetric interface crack and the plane interface crack at the same composite material have the same characteristics of singularity.

Based on Stroh's formulation, Suo et al. (1992) derived the solution for plane problem of an impermeable interface crack in general anisotropic piezoelectric bimetals in the form

$$h(z) = \mathbf{w}z^{-1/2+i\gamma} \quad (5.8)$$

which satisfies the Hilbert problem

$$\bar{\mathbf{H}}\mathbf{w} = e^{2\pi\gamma}\mathbf{H}\mathbf{w} \quad (5.9)$$

where  $\mathbf{H}$  depends upon the material constants.

The Hilbert problem of equation (5.9) can be reduced to the eigenvalue problem given by

$$(\mathbf{D}^{-1}\mathbf{W} + i\beta\mathbf{I})\mathbf{w} = 0, \quad \|\mathbf{D}^{-1}\mathbf{W} + i\beta\mathbf{I}\|\mathbf{w} = \beta^4 + 2b\beta + c = 0 \quad (5.10a)$$

$$\gamma = -[\tanh^{-1}(\beta)]/\pi, \quad b = \left\{ \text{tr} \left[ (\mathbf{D}^{-1}\mathbf{W})^2 \right] \right\} / 4, \quad c = \|\mathbf{D}^{-1}\mathbf{W}\| \quad (5.10b)$$

where

$$\mathbf{D} = \text{Re}[\mathbf{H}], \quad \mathbf{W} = \text{Im}[\mathbf{H}], \quad \mathbf{H} = \mathbf{Y}_1 + \bar{\mathbf{Y}}_2, \quad \mathbf{Y} = i\mathbf{A}\mathbf{B}^{-1} \quad (5.10c)$$

The matrices  $\mathbf{A}$  and  $\mathbf{B}$  are depending upon the material constants. Denoting the real and imaginary roots of the characteristic equation (5.10a) by

$\pm\varepsilon$  and  $\pm\kappa$  respectively, where both  $\varepsilon$  and  $\kappa$  are real numbers and are expressed by

$$\varepsilon = \left\{ \tanh^{-1} \left[ (b^2 - c)^{1/2} - b \right]^{1/2} \right\} / \pi, \quad \kappa = \left\{ \tanh^{-1} \left[ (b^2 - c)^{1/2} + b \right]^{1/2} \right\} / \pi \quad (5.11)$$

With four distinct eigenvalues  $\varepsilon$ ,  $-\varepsilon$ ,  $i\kappa$ ,  $-i\kappa$  and four linearly independent eigenvectors  $w_1$ ,  $\bar{w}_1$ ,  $w_3$ ,  $w_4$ , where  $w_3$  and  $w_4$  are real vectors, the solution can be written as

$$\mathbf{h}(z) = h_1 \mathbf{w}_1 z^{-1/2+i\varepsilon} + h_2 \bar{\mathbf{w}}_1 z^{-1/2-i\varepsilon} + h_3 \mathbf{w}_3 z^{-1/2-\kappa} + h_4 \mathbf{w}_4 z^{-1/2+\kappa} \quad (5.12)$$

where  $h_1$ ,  $h_2$ ,  $h_3$  and  $h_4$  are arbitrary complex constants. The crack-tip stress field can then be obtained as

$$[\sigma_{2i}] = [\sigma_{21}, \sigma_{22}, \sigma_{23}, D_2] = 2 \operatorname{Re}[\mathbf{h}(z)] \quad (5.13)$$

A reduced class from the generalized anisotropic piezoelectric materials is the transversely isotropic piezoelectric (TIP) materials, which is more practical significance, because most of piezoelectric materials commercially used today can be classified into this category. For the interface crack perpendicular to the poling direction of TIP bimetals, it has been shown that one of the two parameters  $\varepsilon$  and  $\kappa$  vanishes (Ou, 2003; Ou and Chen, 2004). When the order of stress singularity is such that  $\varepsilon \neq 0$ , the displacement becomes oscillatory near  $r=0$  and the two crack surfaces penetrate each other. This is a physically unacceptable phenomenon, although the region of penetration is rather small (England, 1965; Erdogan and Gupta, 1972). There have been several studies on the problem to eliminate the unrealistic oscillatory phenomenon by introducing a contact zone near the crack tip (Comninou, 1977; Govorukha and Loboda, 2000; Herrmann et al. 2001; Herrmann and Loboda, 2003). Nevertheless, the calculation show that the singularity indices and for interface crack at a piezoelectric composite are relatively small compared to the classical 1/2 singularity (Ou, 2003; Ou and Chen, 2004). The classical square root singularity

is therefore the dominate term for an interface crack and the singularity index and can be treated as zero for practical applications.

It should be noted that not all inteface crack have the interpenetration problem. By considering equations (5.10)–(5.11),  $\varepsilon = 0$  if  $\mathbf{W} = \mathbf{0}$  or  $\mathbf{H}$  is real. The non-complex ( $\varepsilon = 0$ ) singularity for interface crack happens when some conditions or symmetry are met. For interface crack in isotropic bimaterial, the non-complex singularity occurs when the value of  $(1-2\nu)/\mu$  for the two materials are identical (Ting, 1986). It can be proved that the interface crack parallel to the principal material direction has a classical (non-complex) singularity (Suo et al., 1992; Xu and Rajapakse, 2000b). In the present study, the extended field intensity factors for the axisymmetric cylindrical crack at the interface of a piezocomposite are defined by

$$K_I = \lim_{z \rightarrow c} \sqrt{2\pi(z-c)} (\sigma_{rr}) \Big|_{r=a} \quad (5.14a)$$

$$K_{II} = \lim_{z \rightarrow c} \sqrt{2\pi(z-c)} (\sigma_{rz}) \Big|_{r=a} \quad (5.14b)$$

$$K_D = \lim_{z \rightarrow c} \sqrt{2\pi(z-c)} (D_r) \Big|_{r=a} \quad (5.14c)$$

Note that the mode III deformation vanishes for the axisymmtric crack problem. A comprehensive treatment of electroelastic singularities in multi-material piezoelectric wedges and junctions for elastic anisotropic solids can be found in Xu and Rajapakse (2000b).

#### 5.1.4 DDM Crack Tip Element

The modeling of a crack tip is an important key for the determination of field intensity factors in fracture mechanics. A corollary of the  $r^{-1/2}$  variation in stress near the crack tip is that the relative displacement between the crack surfaces is proportional to  $r^{1/2}$  close to the tip, where  $r$  is measured from the tip along the crack. This requirement encourages us to introduce a special element at the crack tip to replace a constant displacement discontinuity element. The

schematic of the DDM crack tip element is shown in Figure 5.4. The displacement discontinuity functions for a special crack tip element used in the present model can be expressed by

$$\hat{u}_i(z) = u_i^f(a, z) - u_i^m(a, z) = d_i(z/a)^{1/2}, \quad 0 \leq z \leq 2h, \quad i = r, z \quad (5.15)$$

where  $\hat{u}_i$  ( $i = r, z$ ) is the relative displacement between the crack surface and  $2h$  is the length of the crack tip element.

The fundamental solution corresponding to the crack tip displacement discontinuity functions can be determined by replacing equation (5.3a) by (5.15) and solving the relevant boundary-value problem. The crack tip element is implemented in the DDM formulation at each end of the discretized element by substituting the influence coefficients,  $A_{rr}^{ij}$ ,  $A_{rz}^{ij}$ ,  $A_{zr}^{ij}$  and  $A_{zz}^{ij}$ , in equation (5.2) by the corresponding crack tip influence functions for  $i = 1$  and  $i = N$ .

## 5.2 Numerical Results and Discussion

A computer code based on the DDM formulation presented in the preceding section has been developed to study the problem of interface cracks in piezocomposites (Figure 5.1). The required influence functions for the interface dislocation are obtained by evaluating the inverse Fourier integral transform, defined in equation (3.9b), with respect to  $\xi$ . A globally adaptive numerical quadrature scheme is employed to evaluate the integrals. For the purpose of numerical evaluation, the modified Bessel functions  $I_n(x)$  and  $K_n(x)$  appeared in the integrand are evaluated by using the scaled modified Bessel functions  $\hat{I}_n(x)$  and  $\hat{K}_n(x)$  defined by (Abramowitz and Stegun, 1970)

$$\hat{I}_n(x) = e^{-x} I_n(x) \quad (5.16a)$$

$$\hat{K}_n(x) = e^x K_n(x) \quad (5.16b)$$

### 5.2.1 Comparison with Existing Solutions

The validity and accuracy of the present formulation is first verified by comparing with the solutions reported by Kasano et al. (1984) for a cylindrical crack in a transversely isotropic elastic body. Their results correspond to a constant pressure on the crack surfaces for E.glass/epoxy and graphite/epoxy composites and isotropic material with the elastic constants given in Table 5.1 where  $E$ ,  $G$  and  $\nu$  represent the longitudinal and transverse moduli and Poisson's ratio in the plane of isotropic respectively, while  $E'$ ,  $G'$  and  $\nu'$  are the corresponding properties in the principal material direction. A material with same elastic properties as Kasano et al. (1984) is selected and the piezoelectric constants are set to negligibly small values in the present scheme.

Figure 5.5 shows a comparison of crack opening displacements,  $c_{44}^f d_r / pa$ , for a pressurized crack with different crack length  $c/a = 0.1, 1$  and  $10$ . The solutions shown in Figure 5.5 are in good agreement for various types of materials and different values of  $c/a$ . The comparison of solutions for the stress intensity factors  $K_I / p\sqrt{\pi c}$  and  $K_{II} / p\sqrt{\pi c}$  obtained from the present study and those presented by Kasano et al. (1984) is shown in Figure 5.6. Very close agreement is obtained between the two sets of results. Note that electric displacement intensity factor is zero in this case.

The interface cylindrical crack in elastic fiber embedded in an infinite matrix of different elastic materials was considered by Erdogan and Ozbek (1969). The elastic constants for the fiber are  $E^f = 1.0 \times 10^7$  psi and Poisson's ratio  $\nu = 0.20$ , and for the matrix are  $E^m = 4.5 \times 10^5$  psi and  $\nu = 0.35$ . The mode I and II stress intensity factors with  $a/c$  presented by Erdogan and Ozbek (1969) are compared with the present study as shown in Figure 5.7. Once again, very good agreement between the two solutions confirms the accuracy of the present scheme at the limiting case of an ideal elastic composite.

### 5.2.2 Interface Cracks in Piezocomposites

The numerical results corresponding to the cylindrical crack along the interface of the piezocomposite as shown in Figure 5.1 is presented in this section. The fiber and matrix is perfectly bonded except along the crack surfaces ( $-c < z < c$ ) where the constant pressure “ $p$ ” is applied. The boundary condition along the piezoelectric fiber interface is assumed to be electrically impermeable. Two types of piezocomposites are used in the numerical study, i.e., PZT–6B/Matrix A and PZT–6B/Matrix B. The material properties for PZT–6B, Matrix A and Matrix B are given in Table 4.1.

Figure 5.8 presents the crack opening displacement  $c_{44}^f d_r / pa$  for different crack-length, i.e.,  $c/a = 0.1, 0.5, 1, 2, 5$  and  $10$ . The displacement has the largest values at the center of the crack surfaces. The value of maximum displacements at the center increases when the crack-length increases. In addition, the profiles of the crack opening displacement in the region close to the center of the crack surface is more uniform when the crack-length increases. For  $c/a = 10$ , the displacement profiles are almost constant within the region  $-6 < z/a < 6$ . The opening displacement for piezocomposite with Matrix A is larger by 10–20% than that of Matrix B for the specific crack-length. The difference in crack opening displacements between the two composites increases when the crack-length increases.

The variations of field intensity factors  $K_I / p\sqrt{\pi c}$ ,  $K_{II} / p\sqrt{\pi c}$  and  $K_D / p\sqrt{\pi c}$  with crack-length are presented in Figure 5.9. When the crack-length is sufficiently small ( $c/a \rightarrow 0$ ), the solutions approach the plane strain solutions where Mode I stress intensity factor is independent of the material properties and  $K_{II}$  vanishes. For non-zero crack-length, all three intensity factors  $K_I$ ,  $K_{II}$  and  $K_D$  do not vanish. The magnitudes of  $K_I / p\sqrt{\pi c}$  and  $K_D / p\sqrt{\pi c}$  decrease with increasing crack-length while the variation of  $K_{II} / p\sqrt{\pi c}$  increases from zero for  $c/a = 0$  and then gradually decreases for  $c/a > 1$ . Note that  $K_{III}$  vanishes for an

axisymmetric crack problem. In addition, it is observed from Figure 5.9 that the mode II intensity factor is considerably small for a cylindrical interface crack under a constant pressure when compared to  $K_I$  and  $K_D$ .

Table 5.1 Material properties used by Kasano et al. (1984)

	$E'/E$	$G'/G$	$\nu$	$\nu'$
E.glass/Epoxy	16.8	13.9	15.0	0.2827
Graphite/Epoxy	16.3	11.5	14.6	0.2827
Isotropic	3.4	5.62	11.15	0.0



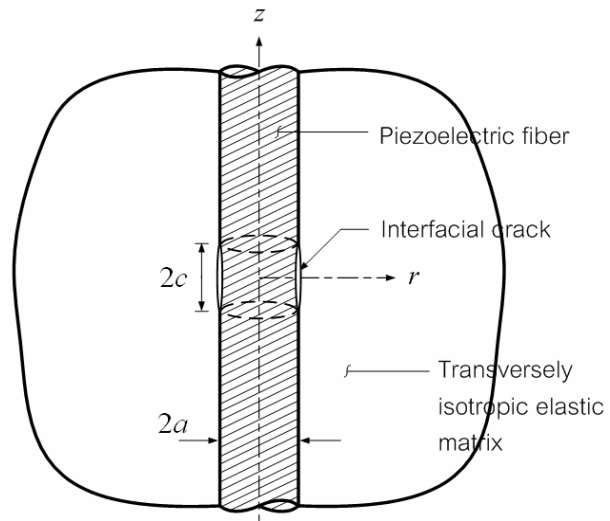


Figure 5.1 A piezoelectric fiber-reinforced composite with interface crack.

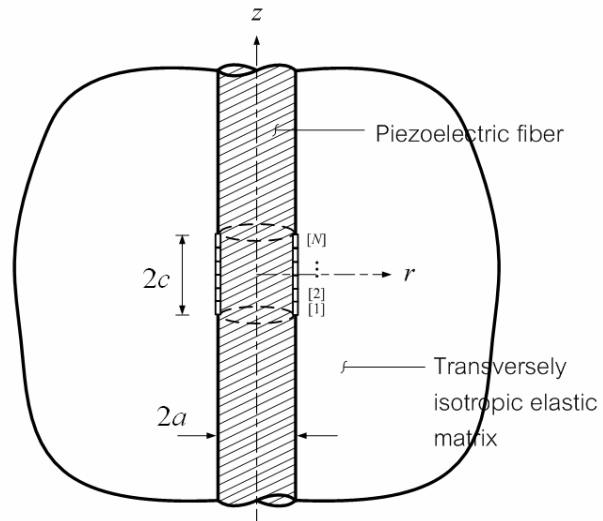


Figure 5.2 Discretization of crack surface into  $N$  segments.

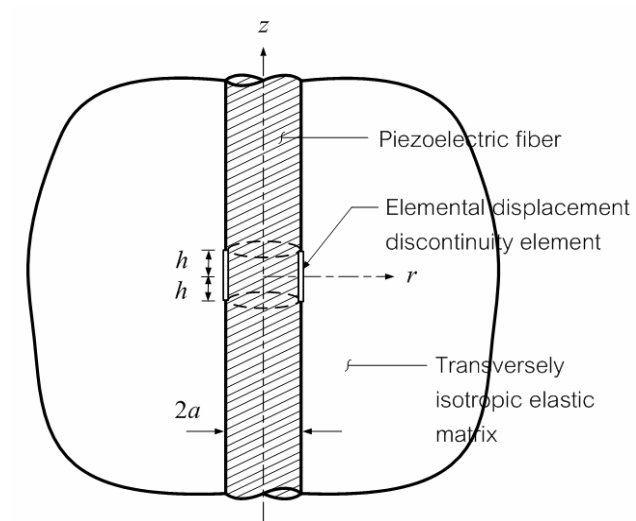


Figure 5.3 A piezocomposite with an elemental displacement discontinuity element.

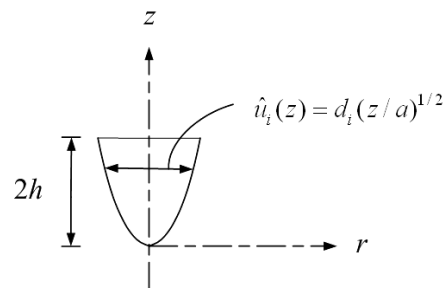


Figure 5.4 DDM crack tip element.

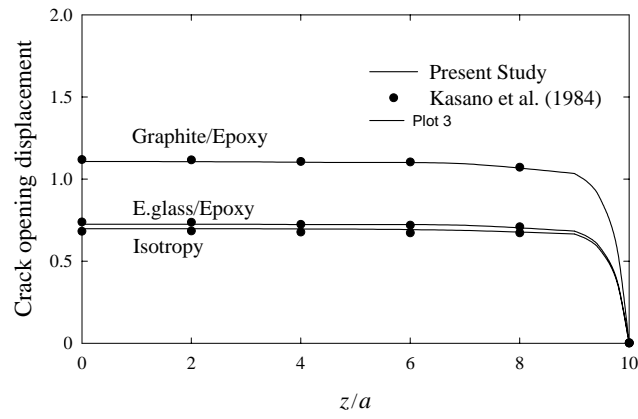
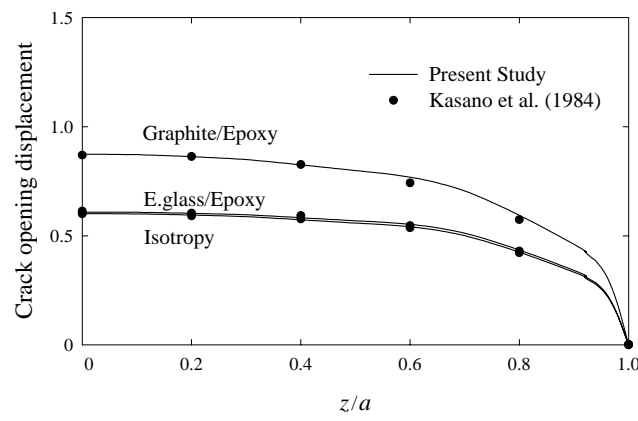
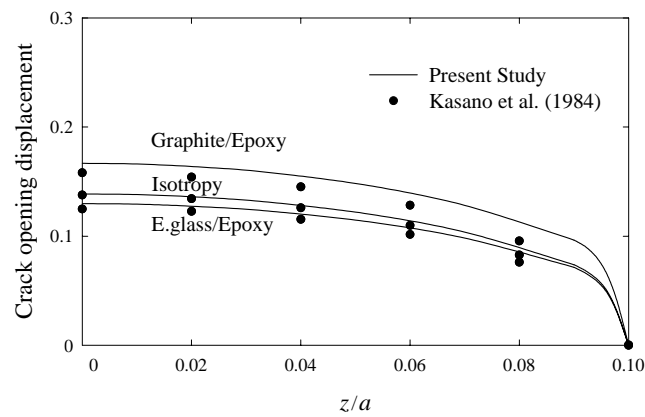
(a)  $c/a = 10$ (b)  $c/a = 1$ (c)  $c/a = 0.1$ 

Figure 5.5 Comparison of crack opening displacement for cylindrical crack in elastic materials.

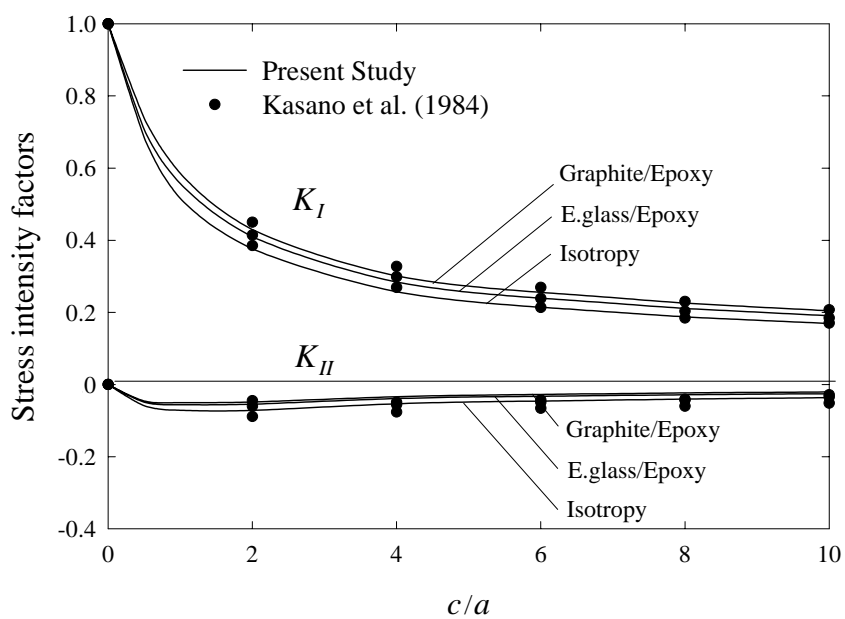


Figure 5.6 Comparison of stress intensity factors for cylindrical crack in elastic materials.

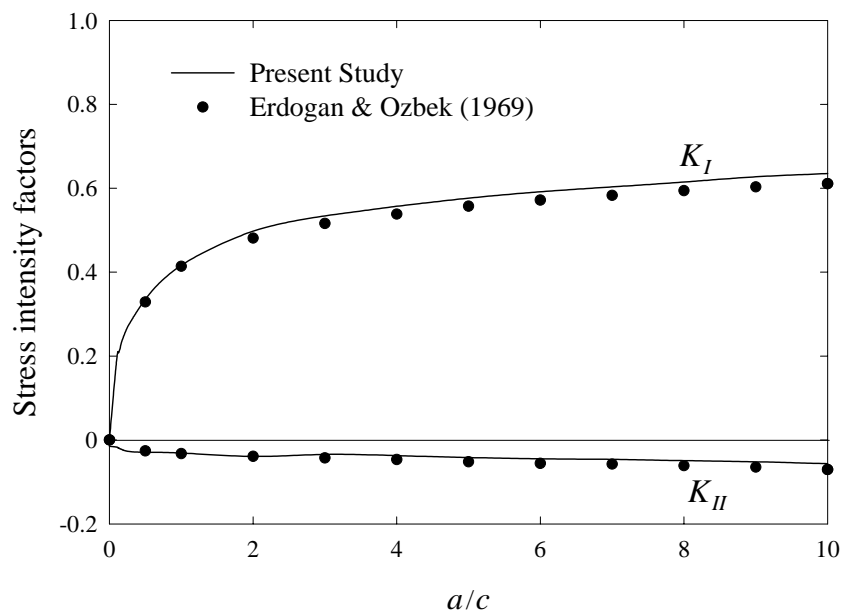


Figure 5.7 Comparison of stress intensity factors for cylindrical interface crack in elastic composite.

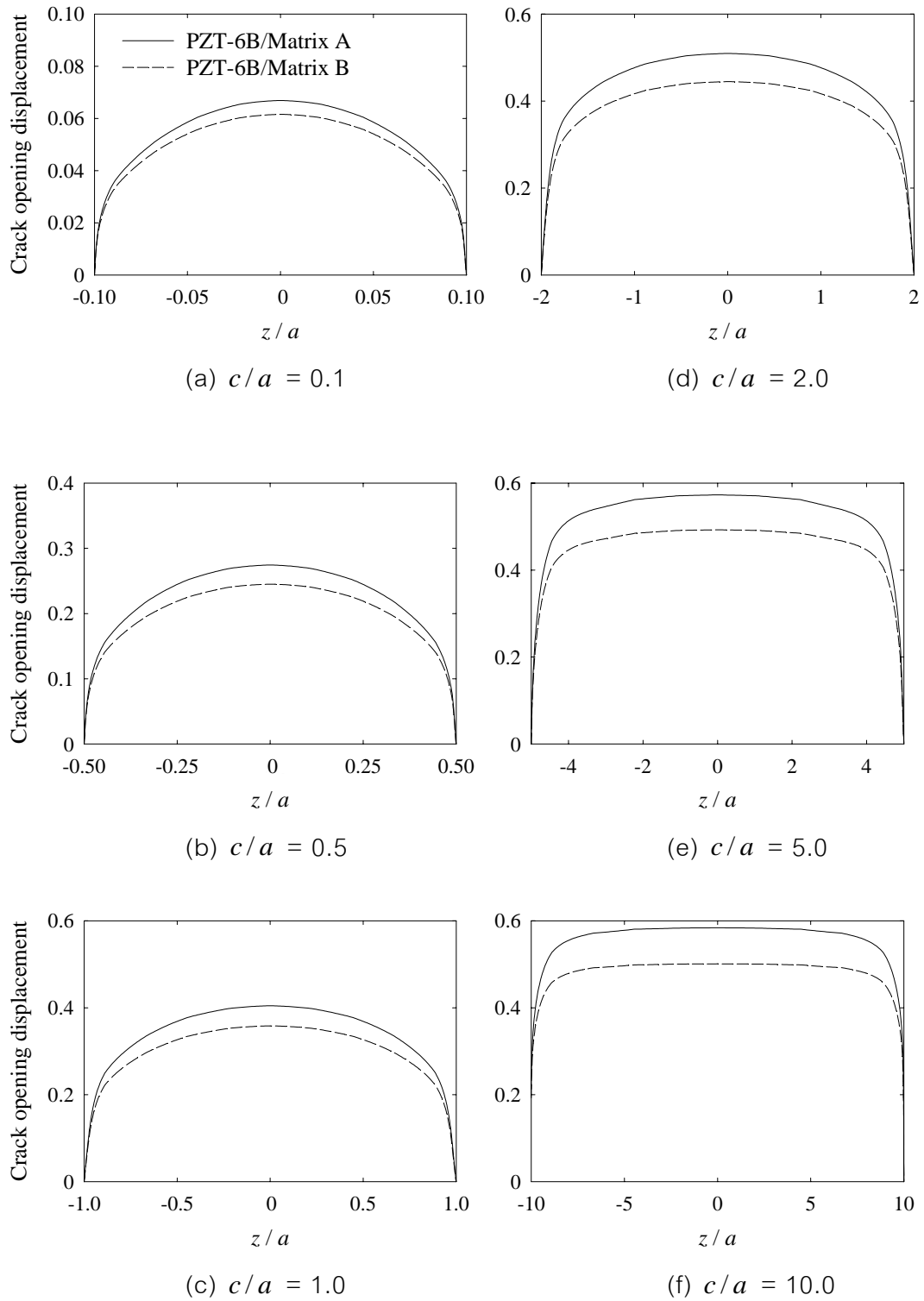


Figure 5.8 Crack opening displacements for cylindrical interface crack in piezocomposites with different  $c/a$ .

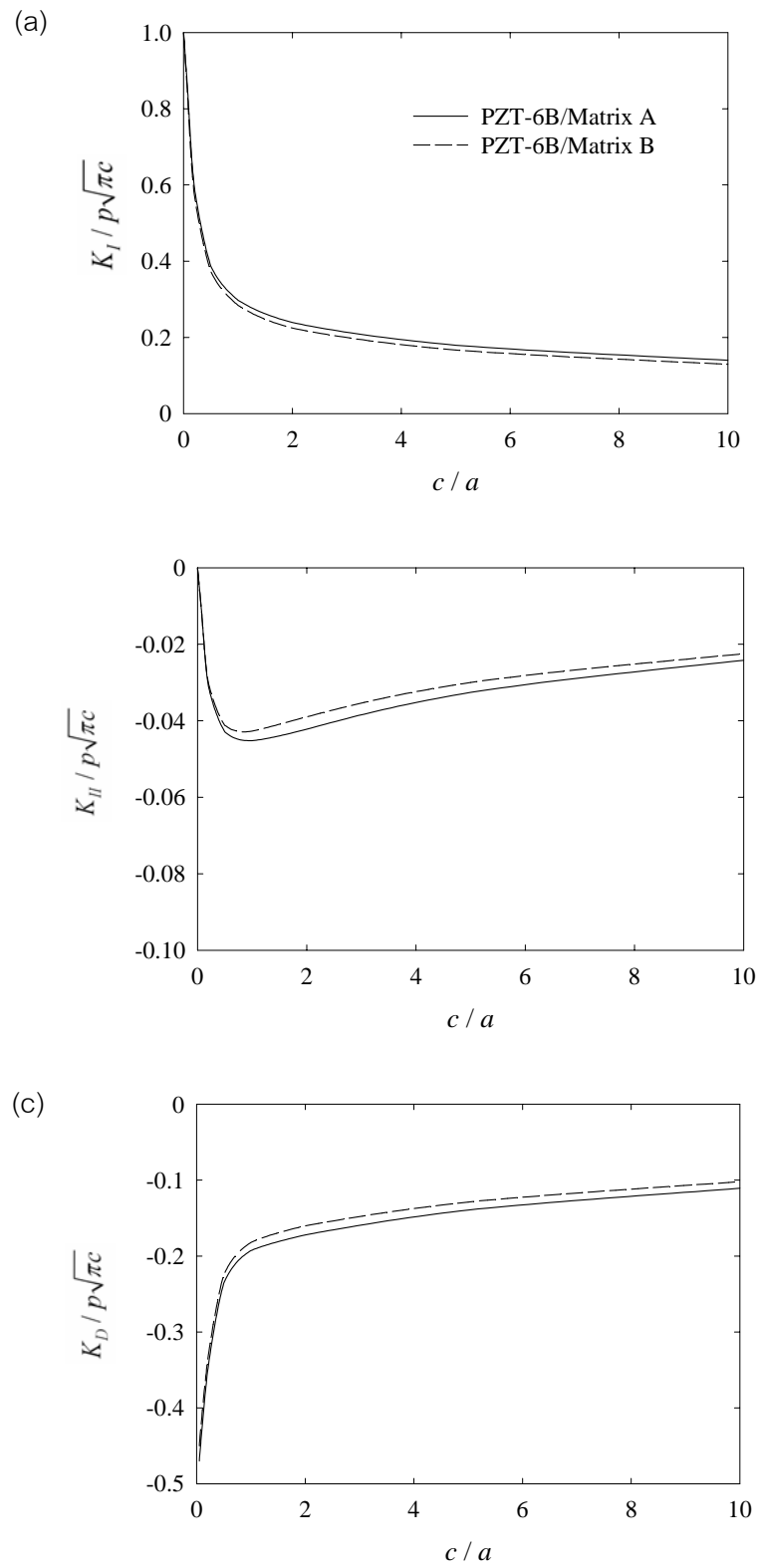


Figure 5.9 Field intensity factors for cylindrical interface crack in piezocomposites.

## CHAPTER VI

### CONCLUSIONS

#### 6.1 Summary

This research presents a comprehensive theoretical study of electroelastic responses of a piezoelectric fiber–reinforced composite with the imperfect interface. The case of an infinitely long cylindrical piezoelectric fiber embedded in a transversely isotropic elastic matrix is considered in the study. Both fiber and matrix are assumed to be transversely isotropic and the principal material directions are in the fiber direction. The main contributions of this research are summarized below.

1. The general solutions for coupled axisymmetric electroelastic fields of a piezoelectric material with a vertical body force and an electric body charge have been derived by using the Fourier integral transforms. The general solutions for piezoelectric materials presented in this work together with the general solutions for a transversely isotropic elastic material are useful for the study of load–transfer mechanisms and interfacial fracture of cylindrical piezoelectric fiber–reinforced composite.

2. The applicability of the general solutions to analyze the boundary–valued problem of electromechanical load transfer and interface dislocations in piezocomposites has been successfully established. For the load transfer problem, the fiber–matrix interface is considered to be either mechanically perfect or imperfect, and either electrically open– or short–circuited. The three–dimensional axisymmetric interfacial cracks in a piezoelectric fiber–reinforced composite is also studied by adopting the displacement discontinuity method (DDM) based on the fundamental solutions of interface dislocation.

3. A computer code based on the formulation for axial load and electric charge transfer and interfacial fracture in piezocomposite has been developed. The validity and accuracy of the solution scheme is confirmed by comparing with the solutions for the limiting case of an ideal elastic material reported in the literature.

4. The effect of various parameters on the axial load and electric charge transfer and interfacial fracture in piezocomposites has been investigated. The major finding concluded from the numerical results are

4.1 The coupled electro–elastic responses in piezoelectric fiber–reinforced composites are very complicated and significantly influenced by the piezoelectric fiber and matrix material properties, the electrical boundary conditions and , the interface conditions such as imperfect fiber–matrix bonding and the presence of interface cracks.

4.2 The stress profiles decrease rapidly in the transverse fiber direction. The magnitude of stresses reduce to relatively small values at  $r/a=4$  which is distance between the adjacent fibers for piezoelectric volume fraction of 20%. This result indicate that the fiber–to–fiber effect has less influence on the composite response and therefore the 1–3 piezocomposite can be modeled by an infinite elastic matrix with a single piezoelectric fiber.

4.3 Under the application of axial load, electric field generated in PZT–4 fiber has the highest values followed by the BaTiO<sub>3</sub> and PZT–6B fibers which implies that PZT–4 is more suitable for applications involving sensing. A softer matrix material result in a higher vertical electric field in the fiber as lesser load is transferred to the matrix. Nevertheless, the fiber axial force and interfacial stresses are primarily controlled by the stiffness of the matrix material and show less dependence on the piezoelectric fiber properties.



4.4 The dependence of interface stresses on the fiber and matrix material type is more pronounced in the case of electric charge loading when compared to the axial loading. Moreover, the vertical stress and electric field show a substantial dependence on the type of piezoelectric fiber.

4.5 The presence of the imperfect interface results in lower axial load transfer to the matrix and hence lower interfacial stresses but a higher fiber vertical electrical field. In the case of electric charge transfer, interfacial stresses decrease and fiber vertical electric field increases as the interface becomes weaker.

4.6 The electric boundary condition (short- or open-circuit) of the fiber shows significant influence on the fiber electric field and interfacial stresses particularly in the electric charge loading case.

4.7 The numerical examples for interface cylindrical crack in piezocomposite show that a crack opening displacement and a stress and electric displacement factors depend on the composite properties and the ratio of crack-length to fiber radius ( $c/a$ ).

4.8 The opening displacement is maximum at the center of the crack surfaces and the value of maximum displacement increases when the crack-length increases. For the limiting case of a vanishingly small crack-length ( $c/a \rightarrow 0$ ), mode I stress intensity factor is independent of the composite material while mode II intensity factor vanishes. The electric displacement intensity factor  $K_D / p\sqrt{\pi c}$  is largest for  $c/a = 0$  and decreases as  $c/a$  increases.

## 6.2 Suggestions for Further Study on Piezocomposites

The results presented in this thesis provide an insight into the fundamental understanding of coupled electroelastic responses in the

composite of piezoelectric materials. The suggestions for further study on mechanics of piezocomposite are

1. The consideration of more complex problems such as composites of piezoelectric fiber with arbitrary cross-section, the interaction of multiple cracks, etc.

2. The study of effective properties of piezoelectric fiber-reinforced composites by employing the micromechanics scheme with the consideration of the effect of piezoelectric fiber volume ratio, fiber and matrix properties and the interface cracks.

## REFERENCES

- Abramowitz, M. and Stegun, I.A. 1970. Handbook of Mathematical Functions. New York : Dover Publications.
- Bent, A.A., Hagood, N.W, and Rodgers, J.P. 1995. Anisotropic actuation with piezoelectric fiber composites. J. Intell. Material. Syst. Structures 6 : 338–349.
- Chen, P.J. 1980. Three–dimensional dynamic electromechanical constitutive relations for ferroelectric materials. Int. J. Solids Structures 16 : 1059–1067.
- Comninou, M. 1977. The interface crack. J. Appl. Mech. 44 : 631–636.
- Crouch, S.L. and Starfield, A.M. 1983. Boundary Element Methods in Solid Mechanics. London : George Allen and Unwin.
- Cruise, T.A. 1988. Boundary element analysis in computational fracture mechanics. Boston : Kluwer academic publishers.
- Deeg, W.F. 1980. The analysis of dislocation, crack and inclusion problems in piezoelectric solids. Ph.D. Dissertation, Department of Materials Science and Engineering, Stanford University.
- Demir, I., Hirth, J.P. and Zbib, H.M. 1992. The extended stress field around a cylindrical crack using the theory of dislocation pile–ups. Int. J. Engng Sci. 31 : 829–845.
- Erdogan, F. and Özbek, T. 1969. Stresses in fibre–reinforced composites with imperfect bonding. J. Appl. Mech. 36 : 865–869.

- Govorukha, V.B. and Loboda, V.V. 2000. Contact zone models for an interface crack in a piezoelectric material. Acta Mechanica 130 : 233–246.
- Gu, B., Liu, H.Y., and Mai, Y.W. 2006. A theoretical model on piezoelectric fibre pullout with electric input. Eng. Fract. Mech. 73 : 2053–2066.
- Hammamia, H., Arousb, M., Lagachea, M. and Kallel, A. 2006. Experimental study of relaxations in unidirectional piezoelectric composites. Composites A 37 : 1–8.
- Herrmann, K.P., Loboda, V.V. and Govorukha, V.B. 2001. On contact zone models for an electrically impermeable interface crack in a piezoelectric biomaterial. Int. J. Fracture 111 : 203–227.
- Herrmann, K.P. and Loboda, V.V. 2003. Fracture mechanical assessment of interface cracks with contact zones in piezoelectric bimetals under thermoelectromechanical loadings I. Electrically permeable interface cracks. Int. J. Solids Structures 40 : 4191–4217.
- Heyer, V., Schneider, G.A., Balke, H., Drescher, J. and Bahr, H.A. 1998. A fracture criterion for conducting cracks in homogeneously poled piezoelectric PZT–PIC151 ceramics. Acta Materialia 46 : 6615–6622.
- Kasano, H., Matsumoto, H. and Nakahara, I. 1984. A torsion-free axisymmetric problem of a cylindrical crack in a transversely isotropic body. Bull JSME. 27 : 1323–1332.
- Kasano, H., Matsumoto, H. and Nakahara, I. 1986. A cylindrical interface crack in a nonhomogeneous anisotropic elastic body. Bull JSME. 29 : 1973–1981.
- Kuriyama, K. and Mizuta, Y. 1993. Three-dimensional elastic analysis by the displacement discontinuity method with boundary division into triangle leaf elements. Int. J. Rock Mech. Min. Sci. Geomech. 30 : 111–123.

- Lekhnitskii, S.G. 1963. Theory of elasticity of an anisotropic elastic body. New York : Holden-Day.
- Lenci, S. and Menditto, G. 2000. Weak interface in long fiber composites. Int. J. Solids Structures 37 : 4239–4260.
- Li, L. and Sottos, N.R. 1996. A design for optimizing the hydrostatic performance of 1–3 piezocomposites. Ferroelect Lett. 21 : 41–46.
- Liu, H.Y., Qin, Q.H. and Mai Y.W. 2003. Theoretical model of piezoelectric fibre pullout. Int. J. Solids Structures 40 : 5511–5519.
- Mal, A.K. and Bose, S.K. 1975. Dynamic elastic moduli of a suspension of imperfectly bonded spheres. Proc. Cambridge Phil. Soc. 76 : 587–600.
- Mindlin, R.D. 1974. Equations of high frequency vibrations of thermopiezoelectric crystal plates. Int. J. Solids Structures 10 : 625–637.
- Montgomery, R.E. and Richard, C. 1996. A model for the hydrostatic pressure response of a 1–3 composite. IEEE Trans. Ultrason. Ferroelect. Freq. Contr. 43 : 457–66.
- Muki, R. and Sternberg, E. 1969. On the diffusion of an axial load from an infinite cylindrical bar embedded in an elastic medium. Int. J. Solids Structures 5 : 587–605.
- Nairn, J.A. and Liu, Y.C. 1996. Stress transfer into a fragmented anisotropic fiber through an imperfect interface. Int. J. Solids Structures 34 : 1255–1281.
- Nelson, L.J. 2002. Smart piezoelectric fibre composites. Mat. Sci. Tech. 18 : 1245–1256.
- Newnham, R.E., Skinner, D.P. and Cross, L.E. 1978. Connectivity and piezoelectric–pyroelectric composites. Mater. Res. Bull. 13 : 525–536.

- Niumpradit, B. and Karasudhi, P. 1981. Load transfer from an elastic pile to a saturated porous elastic soil. Int. J. Numer. and Anal. Meth. Geomech. 5 : 115–138.
- Ou, Z.C. and Wu, X. 2003. On the crack-tip stress singularity of interfacial cracks in transversely isotropic piezoelectric bimetals. Int. J. Solids Structures 40 : 7499–7511.
- Ou, Z.C. and Chen, Y.H. 2004. Interface crack problem in elastic dielectric/piezoelectric bimetals. Int. J. Fracture 130 : 427–454.
- Pak, R.Y.S. and Gobert, A.T. 1993. Axisymmetric problems of a partially embedded rod with radial deformation. Int. J. Solids Structures 29 : 1745–1759.
- Pak, Y.E. 1992. Linear electroelastic fracture mechanics of piezoelectric materials. Int. J. Fracture 54 : 79–100.
- Pan, E. 1999. A BEM analysis of fracture mechanics in 2D anisotropic piezoelectric solids. Engrg. Anal. Bound. Elem. 23 : 67–76.
- Park, S.B. and Sun, C.T. 1995. Fracture criteria for piezoelectric ceramics. J. Am. Ceram. Soc. 78 : 1475–1480.
- Parton, V.Z. and Kudryavtsev, B.A. 1988. Electromagnetoelasticity. New York : Gordon and Breach Science Publishers.
- Piessens, R., Doncker, E., Uberhuber, C., Kahaner, D. 1983. QUADPACK: a subroutine package for automatic integration. Berlin: Springer.
- Rajapakse, R.K.N.D. 1996. Electroelastic response of a composite cylinder with a piezoceramic core. Proceedings of SPIE, California 2715 : 84–94.

- Rajapakse, R.K.N.D. 1997. Plane strain/stress solutions for piezoelectric solids. Composites B 28 : 385–396.
- Rajapakse, R.K.N.D., Chen, Y. and Senjuntichai, T. 2005. Electroelastic field of a piezoelectric annular finite cylinder. Int. J. Solids Structures 42 : 3487–3508.
- Rajapakse, R.K.N.D. and Chen, Y. 2008. A coupled analytical model for hydrostatic response of 1–3 piezocomposites. IEEE Trans. Ultrason. Ferroelect. Freq. Contr. 55 : 1847–1858.
- Rajapakse, R.K.N.D. and Xu, X.L. 2001. Boundary element modeling of cracks in piezoelectric solids. Engng. Analysis Boundary Elem. 25 : 771–781.
- Rajapakse, R.K.N.D. and Zhou, Y. 1997. Stress analysis of piezoceramic cylinders. Smart Mat. Structures 62 : 169–177.
- Rao, S.S. and Sunar, M. 1994. Piezoelectricity and its use in disturbance sensing and control of flexible structures: A survey. Appl. Mech. Rev. 47 : 113–123.
- Selvadurai, A.P.S. and Rajapakse, R.K.N.D. 1990. Axial stiffness of anchoring rods embedded in elastic media. Can. J. Civ. Eng. 173 : 321–328.
- Senjuntichai, T., Sornpakdee, N., Teerawong, J., Rajapakse, R.K.N.D. 2007. Time dependent response of an axially loaded elastic bar in a multi-layered poroelastic medium. J. Engng. Mech., ASCE May : 578–587.
- Senjuntichai, T., Kaewjuea, W. and Rajapakse, R.K.N.D. 2008. Piezoelectric cylinder under voltage and axial loading. Int. J. Appl. Electromagnetics Mech. 47–50 : 789–792.

- Slaughter, W.S. and Sanders, J.L. 1991. A model for the load–transfer from an embedded fiber to an elastic matrix. Int. J. Solids Structures 28 : 1041–1052.
- Sneddon, I. 1970. The use of integral transforms. New York : McGraw–Hill.
- Sosa, H. 1991. Plane problems in piezoelectric media with defects. Int. J. Solids Structures 28 : 491–505.
- Sosa, H. 1992. On the fracture mechanics of piezoelectric solids. Int. J. Solids Structures 29 : 2613–2622.
- Sosa, H. and Pak, Y.E. 1990. Three–dimensional eigenfunction analysis of a crack in a piezoelectric material. Int. J. Solids Structures 26 : 1–15.
- Suo, Z., Kuo, C.M., Barnett, D.M. and Willis, J.R. 1992. Fracture mechanics for piezoelectric ceramics. J. Mechs. Phys. Solids 40 : 739–765.
- Stroh, A.N. 1962. Steady state problems in anisotropic elasticity. J. Mathematics Physics 41 : 77–103.
- Ting, T.C.T. 1986. Explicit solution and invariance of the singularities at an interface crack in anisotropic composites. Int. J. Solids Structures 9: 965–983.
- Wang, Z. and Zheng, B. 1995. The general solution of three–dimensional problems in piezoelectric media. Int. J. Solids Structures 32 : 105–115.
- Watson, G.N. 1972. A treatise on the theory of bessel functions. Cambridge University Press.
- Xu, X.L. and Rajapakse, R.K.N.D. 1999. Analytical solution for an arbitrarily oriented void/crack and fracture of piezoceramics. Acta Materialia 47 :1735–1747.



- Xu, X.L. and Rajapakse, R.K.N.D. 2000a. A theoretical study of branched cracks in piezoelectrics. Acta materialia 48 : 1865–1882
- Xu, X.L. and Rajapakse, R.K.N.D. 2000b. On singularities in composite piezoelectric wedges and junctions. Int. J. Solids Structures 37 : 3253–3275.
- Xu, X.L. and Rajapakse, R.K.N.D. 2001. On a plane crack in piezoelectric solids. Int. J. Solids Structures 38 : 7643–7658.

## APPENDICES

## APPENDIX A

The characteristic roots  $v_j$  appearing in equation (3.10) are determined from the following equation:

$$Av^3 + Bv^2 + Cv + D = 0 \quad (\text{A.1})$$

where the coefficients  $A$ ,  $B$ ,  $C$  and  $D$  are constants expressed in terms of material properties as

$$A = c_{11}^f \left\{ (e_{15}^f)^2 + c_{44}^f \varepsilon_{11}^f \right\} \quad (\text{A.2})$$

$$B = c_{13}^f \left\{ 2e_{15}^f (c_{13}^f + 2c_{44}^f) + \varepsilon_{11}^f (c_{13}^f + 2c_{44}^f) \right\} - c_{11}^f (2e_{15}^f e_{33}^f + c_{33}^f \varepsilon_{11}^f + c_{44}^f \varepsilon_{33}^f) \quad (\text{A.3})$$

$$C = c_{11}^f \left\{ (e_{33}^f)^2 + c_{33}^f \varepsilon_{33}^f \right\} + c_{13}^f \left\{ 2e_{33}^f (e_{15}^f + e_{31}^f) + \varepsilon_{33}^f (c_{13}^f + 2c_{44}^f) \right\} \\ + c_{33}^f (e_{15}^f + e_{31}^f)^2 + c_{44}^f (2e_{31}^f e_{33}^f - c_{33}^f \varepsilon_{11}^f) \quad (\text{A.4})$$

$$D = -c_{44}^f \left\{ (e_{33}^f)^2 + c_{33}^f \varepsilon_{33}^f \right\} \quad (\text{A.5})$$

The three roots of equation (A.1) are denoted by  $v_j$  ( $j = 1, 2, 3$ ) with  $v_1$  assumed to be a positive real number and  $v_2$  and  $v_3$  either positive real numbers or a pair of complex conjugates with positive real parts. The characteristic roots, obtained from equation (A.1), for the piezoelectric materials PZT-6B, PZT-4 and BaTiO<sub>3</sub> (see Table 4.1) are presented in Table A.1 and the characteristic roots for the Matrix A and Matrix B, determined from equation (3.19), are given in Table A.2.

Table A.1 Characteristic roots for piezoelectric materials.

	$v_1$	$v_2$	$v_3$
PZT-6B	(1.9320, 0.0)	(1.9320, 0.0)	(1.9320, 0.0)
PZT-4	(0.8307, 0.0)	(0.9037, 0.1697)	(0.9037, -0.1697)
BaTiO <sub>3</sub>	(1.0631, 0.0)	(0.9468, 0.2162)	(0.9468, -0.2162)

Table A.2 Characteristic roots for Matrix A and Matrix B.

	$w_1$	$w_2$
Matrix A	(2.9308, 0.0)	(0.6073, 0.0)
Matrix B	(1.0720, 0.0)	(0.9328, 0.0)

## APPENDIX B

The functions appearing in equations (5.4)-(5.7) are related to the fiber and matrix 's material properties and defined as

$$I_{mj} = I_m(\xi_j a); \quad K_{mk} = K_m(\xi_k a); \quad (m = 0, 1; \quad j = 1, 2, 3; \quad k = 1, 2) \quad (\text{B.1})$$

$$\begin{aligned} h_{1j} &= c_{11}^f v_j - c_{13}^f k_{1j} - e_{13}^f k_{2j}; \quad h_{2j} = i\xi_j \left[ c_{44}^f (1 + k_{1j}) - e_{15}^f k_{2j} \right] \\ h_{3j} &= i\xi_j \left[ e_{15}^f (1 + k_{1j}) - d_{11}^f k_{2j} \right]; \quad g_j = v_j (c_{12}^f - c_{11}^f) / a; \quad m_j = k_{1j}^h \\ y_{1k} &= c_{11}^m w_k - c_{13}^m n_k; \quad s_k = w_j (c_{12}^m - c_{11}^m) / a \end{aligned} \quad (\text{B.2})$$

$$\begin{aligned} I_{a1} &= I_{12} I_{13}; \quad I_{a2} = I_{11} I_{13}; \quad I_{a3} = I_{11} I_{12} \\ I_{b1} &= I_{03} I_{12}; \quad I_{b2} = I_{03} I_{11}; \quad I_{b3} = I_{02} I_{11} \\ I_{c1} &= I_{02} I_{13}; \quad I_{c2} = I_{01} I_{13}; \quad I_{c3} = I_{01} I_{12} \\ I_{d1} &= I_{01} I_{12} I_{13}; \quad I_{d2} = I_{02} I_{11} I_{13}; \\ I_{d3} &= I_{03} I_{11} I_{12}; \quad I_e = I_{11} I_{12} I_{13} \end{aligned} \quad (\text{B.3})$$

$$K_a = K_{02} K_{11}; \quad K_b = K_{01} K_{12}; \quad K_c = K_{01} K_{02}; \quad K_d = K_{11} K_{12} \quad (\text{B.4})$$

$$\begin{aligned} h_{a1} &= h_{22} h_{33} - h_{23} h_{32}; \quad h_{a2} = h_{21} h_{33} - h_{23} h_{31}; \quad h_{a3} = h_{21} h_{32} - h_{22} h_{31} \\ h_{b1} &= h_{12} h_{33} - h_{13} h_{32}; \quad h_{b2} = h_{11} h_{33} - h_{13} h_{31}; \quad h_{b3} = h_{11} h_{32} - h_{12} h_{31} \end{aligned} \quad (\text{B.5})$$

$$\begin{aligned} p_{a1} &= g_2 h_{33} - g_3 h_{32}; \quad p_{a2} = g_1 h_{33} - g_3 h_{31}; \quad p_3 = g_1 h_{32} - g_2 h_{31} \\ p_{b1} &= m_2 h_{33} - m_3 h_{32}; \quad p_{b2} = m_1 h_{33} - m_3 h_{31}; \quad p_{b3} = m_1 h_{32} - m_2 h_{31} \\ p_{c1} &= g_2 h_{23} - g_3 h_{22}; \quad p_{c2} = g_1 h_{23} - g_3 h_{21}; \quad p_{c3} = g_1 h_{22} - g_2 h_{21} \end{aligned} \quad (\text{B.6})$$

$$\begin{aligned} \beta_1 &= |\xi| I_e (h_{a1} v_1 + h_{a2} v_2 + h_{a3} v_3) \\ \beta_2 &= |\xi| I_e (p_{a1} v_1 + p_{a2} v_2 + p_{a3} v_3) \end{aligned} \quad (\text{B.7})$$

$$\begin{aligned}
\gamma_1 &= K_a n_2 s_1 - K_b n_1 s_2 + |\xi| K_c (n_2 y_{11} - n_1 y_{12}) + I_{02} I_{01} I_{13} h_{23} (k_{12} h_{11} - k_{11} h_{12}) \\
\gamma_2 &= n_2 y_{21} K_a - |\xi| n_1 y_{22} K_b \\
\gamma_3 &= (s_2 y_{21} - s_1 y_{22}) K_d + |\xi| (y_{12} y_{21} K_a - y_{11} y_{22} K_b) \\
\gamma_4 &= |\xi| (h_{11} h_{a1} I_{d1} + h_{12} h_{a2} I_{d2} + h_{13} h_{a3} I_{d3}) \\
\gamma_5 &= I_e (h_{31} p_{c1} + h_{32} p_{c2} + h_{33} p_{c3}) \\
\gamma_6 &= I_{d1} m_1 h_{a1} + I_{d2} m_2 h_{a2} + I_{d3} m_3 h_{a3} \\
\gamma_7 &= |\xi| (K_a w_1 z_{12} - K_b w_2 z_{11}) + K_d (s_2 w_1 - s_1 w_2) \\
\gamma_8 &= (h_{33} v_2 - h_{32} v_3) \left[ |\xi| (z_{12} z_{21} K_a - z_{11} z_{22} K_b) + K_d (s_2 z_{21} - s_1 z_{22}) \right]
\end{aligned} \tag{B.8}$$

## BIOGRAPHY

The author, Yasothorn Sapsathiarn, was born in Ayutthaya, Thailand, on March 1, 1977. He received his Bachelor of Engineering degree in Civil Engineering from Chulalongkorn University in 1998 with the support from Chula-Chonnabot Scholarship. He continued his Master degree study at Chulalongkorn University in the same year under the supervision of Associate Professor Dr.Teerapong Senjuntichai and successfully fulfilled the requirements for the M.Eng. degree in April of 2001. He was employed as a design engineer at Meinhardt (Thailand) company until April of 2004 and enrolled in Chulalongkorn University to pursue a Doctor of Philosophy degree in Civil Engineering, again with Dr.Teerapong Senjuntichai, in May of 2004 under the Royal Golden Jubilee Scholarship from Thailand Research Fund. He spent the summers of 2007 and 2008 at the University of British Columbia, Vancouver, Canada, to conduct a research work with Professor Dr.Nimal Rajapakse.